Differential Equations and Dynamical Systems
https://doi.org/10.1007/s12591-023-00667-6

ORIGINAL RESEARCH

Dynamics of CoVid-19 Disease in Semarang, Indonesia: Stability, Optimal Control, and Model-Fitting

Mohammad Ghani[1] · **Yolanda Norasia**[2] · **Wahyuni Ningsih**[3]

Accepted: 30 October 2023

Abstract
The dynamics of CoVid-19 disease becomes a concern in this paper. Initially, the positivity and boundedness are established to ensure that the number of susceptible, infected, quarantined, and recovered individuals are always positive in the population and the population numbers are always bounded. The equilibrium points of disease-free and endemic are then determined for uncontrolled dynamical system. Based on the equilibrium points, we can provide the basic reproduction number to ensure that infectious disease can transmit or not in the population. The infection has ability to transmit in the population if $\mathcal{R}_0 > 1$ and vice versa. The local stability is established through the Jacobian matrix at the disease-free and endemic equilibrium points. The appropriate Lyapunov function is initially introduced to provide the global stability of dynamical system. Moreover, the sensitivity analysis is used to determine the dominant parameters for each state variable (most positive or negative). The least square technique is used to compare the numerical results using the fourth-order Runge–Kutta and actual data of CoVid-19 disease in Semarang, Indonesia. Moreover, Continuous Time Markov Chain (CTMC) gives the same patterns between the deterministic and stochastic results. Because vaccination and social distancing have a significant impact on the profile of susceptible, infected, quarantined, and recovered classes, then we introduce a mathematical model of CoVid-19 with two time-dependent controls $(u_1, u_2)(t)$. It follows from the results obtained, the implementation of control gives the number of infected, quarantined, and recovered individuals decreased, and the number of susceptible individuals increased. The neural network approach also gives the significant estimations based on the root mean square error by using the training function of Levenberg-Marquadt.

Keywords Basic reproduction number · Optimal control · Vaccination · Social distancing · Least square technique · CoVid-19 disease · Continuous time markov chain · Neural network · Levenberg–Marquadt

Mathematics Subject Classification 35A01 · 35B40

✉ Mohammad Ghani
mohammad.ghani2013@gmail.com

[1] Faculty of Advanced Technology and Multidiscipline, Universitas Airlangga, Surabaya 60115, Indonesia

[2] Department of Mathematics, Universitas Islam Negeri Walisongo, Semarang 50185, Indonesia

[3] Department of Chemical Engineering, Politeknik Negeri Malang, Malang 65141, Indonesia

Introduction

Covid-19 originated from a coronavirus that has been endemic since 2019. Coronaviruses can spread through the air and can cause fever and shortness of breath. In Indonesia, Covid-19 spread for the first time on March 2, 2020 [25]. The Covid-19 epidemic has not yet ended. In data sourced from covid.19.go.id there are 14,657 active cases of covid-19 in Indonesia. The Ministry of Health has appealed to the public to actively use masks again to prevent a potential spike in Covid-19 cases. The increase in Covid-19 was due to a new variant of Covid-19 that entered Indonesia, namely the Arcturus variant. This variant causes fever, cough, muscle aches, and also conjunctivitis. In January 2023, the Arcturus variant was discovered for the first time in India. To form Arcturus, two or more sublineages underwent homologous recombination [34]. Sourced from the Ministry of Health, cases of the Arcturus variant of Covid-19 increased in mid-April 2023 in Indonesia. Predicting the spread of disease outbreaks can be studied through applied mathematics. The *SI* (Susceptible-Infection) simple mathematical model is applied to Covid-19's spread. The *SI* model involves the Bernoulli Verhulst model to derive an identification parameter approach [24]. Predicting the number of population requiring medical treatment can use the *SIR* model with Susceptible-Infection-Recovered during Covid-19's spread pandemic [3]. By combining the Lyapunov method and the LaSalle invariant principle, the Covid-19 model with *SIR* considers the effect of room availability at the hospital and reduces the spread of Covid-19 [7]. Using the classic Kermack-McKendrick model, this study examines the spread of Covid-19. Additionally, the *SIR* model was applied to the first wave of Covid-19 spreading in Malaysia. This study shows that control in the form of awareness of cleanliness and social distancing can reduce the transmission of Covid-19 [9]. With appropriate restrictions and strong policies, the *SIR* model of Covid-19's spread can be controlled in all communities based on the data recorded and the data from the modeling approach [23]. The *SIR* model for individuals I and R depends on the parameters of the level of interaction and the intensity of the patient's recovery [33]. The Convex event rate at *SIR* was solved numerically using the Non-Standard Finite Difference (NSFD) method [45]. In a short-term comparison of the Covid-19 spread model to the *SIR*, Verhulst, and Gompertz models, the SIR is found to be more useful [26]. The spread of Covid-19 in the *SIR* model based on the influence of the health system shows local stability when the reproductive number is less than one [4].

A model for predicting Covid-19's spread in the short and long-term was based on four compartments, namely *SIRD* (susceptible-infection-recovered-decreased) [12]. The *SIRD* model is a nonlinear differential equation used to predict Covid-19 infection in the short term [36]. A model called *SIRD* (susceptible-infection-recover-dead) was implemented in Indonesia to estimate the Covid-19's spread in the long term [37]. When the *SIRD* is used to predict Covid-19's spread with sex and age filters, it shows that the younger population is more likely to infect the older population [13]. Covid-19 is an epidemic that can occur in any country, according to the *SIRD* model, with a reproduction number ranging from 1.0011 to 2.7936 [6]. In the case of Covid-19, there are exposed individuals, namely individuals who are not necessarily positive but experience symptoms of Covid-19. The addition of the exposed subpopulation to the SEIR model shows the need for control to reduce the impact of Covid-19 [30]. The *SEIR* considering vaccination and isolation for the Covid-19 case shows an increase in the recovered population in Indonesia [8]. The Adaptive *SIRV* Model ($A - SIRV$) is time-dependent for estimating the spread of the Covid-19 outbreak using the Variational Imbedding method [35]. Vaccination against Covid-19 is not only done once. Research on mathematical models with the first and second vaccinations was conducted by Sepulveda et al. The study

describes the behavior of Covid-19 after the initial vaccination [43]. The *SVIR* (susceptible-vaccine-infection-removed) mathematical model assumes that susceptible individuals will be vaccinated. This study uses the ordinary least squares in the SVIR model [40]. Vaccine allocation based on the highest spread of Covid-19 can increase the benefits of the vaccination program in Indonesia [28]. Even though they have implemented vaccinations, it is undeniable that susceptible individuals can be re-exposed to Covid-19. One of the efforts to prevent the spread is to implement quarantine for individuals exposed to Covid-19. A *SIQR* model is a Covid-19 model that consists of four compartments: susceptible, infection, quarantine, and recovery [38]. The *SIQR* model is suitable for areas that have implemented quarantine rules. According to research on the *SIQR* model, large noise can cause the disease to disappear exponentially, establishing sufficient conditions for a unique stationary distribution to exist [15]. The *SIQR* model with the Atangana-Beleanu-Caputo (ABC) fractional fractal derivative was applied in the spread of Covid-19 conducted by Adnan et al. This research shows that quarantine is able to control the spread of Covid-19 [1]. The nonstandard finite difference (NSFD) numerical solution applied to the *SIQR* model of the spread of Covid-19 provides a positive and convergent solution towards stability [2]. With the new Arcturus Covid-19 variant entering Indonesia, it is necessary to provide preventive measures in the form of quarantine. It is of interest to researchers to see how Covid-19 spreads concerning quarantine, which reduces the risk of individuals contracting the infection. In this study, a model of Covid-19 spread is presented with strategic control of social restrictions, observing both local and global stability of disease-free and endemic areas. The other studies of the latest progress in this research field can be referred to [10, 11, 17–20, 31, 39, 44].

Other parts of this paper are organized as follows. Section 1 provides the introduction of this study. The model formulation and also the theorems of positivity, boundedness, existence, and uniqueness are given in Section 2. Section 3 presents equilibria points, basic reproduction number, local stability, and global stability at the equilibria points. Due to the effectiveness of control for our dynamical system, the optimal control is introduced in Section 4. Section 5 gives the numerical results and discussion consisting of sensitivity analysis, simulation of *SIQR* model, best fit parameters using least square technique, comparison results between deterministic and stochastic *SIQR* models using continuous time markov chain, simulation of *SIQR* model with optimal control, and also the estimation results by using neural network, where the training function of Levenberg-Marquardt and activation function of Tangent Sigmoid are employed for the best model of neural network. Finally, the conclusions of this study are established in Section 6.

Mathematical Model

We firstly consider the following SIQR model on CoVid-19 disease without a control strategy

$$\begin{aligned}
\frac{dS}{dt} &= \Lambda - \beta\delta SI - \mu S,\\
\frac{dI}{dt} &= \beta\delta SI - (r + \epsilon + \mu + d)I,\\
\frac{dQ}{dt} &= \epsilon I - (\varphi + d + \mu)Q,\\
\frac{dR}{dt} &= rI + \varphi Q - \mu R,
\end{aligned} \tag{2.1}$$

where the notations and values in system (2.1) are shown in Table 1 and the state variables S, I, Q, R respectively represent the susceptible, infected, quarantined, and recovered sub populations. The dynamical system (2.1) is a modification of mathematical model introduced by Crokidakis [21, 22], by introducing the lockdown δ and isolation rate ϵ. Moreover, we validate our system (2.1) by comparing the numerical results using fourth-order Runge–Kutta and actual data of CoVid-19 in Semarang, Indonesia. Due to the effectiveness of control implementation for our model of dynamical system, then we also introduce two controls including the vaccination and social distancing.

Remark 1 In epidemiology, the main concern is to reduce the number of infected individuals. Based on the previous studies in [21, 22], then our contributions of this paper are to introduce the lockdown δ ($\delta \in (0, 1]$, there is no lockdown when $\delta = 1$, and full lockdown is when $\delta = 0$) and isolation rate ϵ, where these two strategies are effective enough to reduce the transmission number of CoVid-19. Moreover, the time-dependent optimal controls of vaccination u_1 and social distancing u_2 are also provided to degrade the CoVid-19 transmission in the population.

Theorem 1 *Let the initial conditions of system* (2.1) $(S, I, Q, R)(0)$ *be positive, then the solutions* $(S, I, Q, R)(t)$ *of system* (2.1) *are also positive for every* $t > 0$.

Proof For first state variable of (2.1), one has

$$\frac{dS}{dt} = \Lambda - H(t)S(t), \tag{2.2}$$

where $H(t) = \beta\delta I(t) + \mu$. Multiplying the above result by the term

$$\exp\left(\int_0^t H(\xi)d\xi\right).$$

Then one can obtain

$$\frac{dS}{dt} \cdot \exp\left(\int_0^t H(\xi)d\xi\right) = (\Lambda - H(t)S(t)) \cdot \exp\left(\int_0^t H(\xi)d\xi\right),$$

implying that

$$\frac{d}{dt}\left(S(t) \cdot \exp\left(\int_0^t H(\xi)d\xi\right)\right) = \Lambda \cdot \exp\left(\int_0^t H(\xi)d\xi\right).$$

By taking the integration with respect to t, one has

$$S(t) = \left(S(0) + \int \Lambda \cdot \exp\left(\int_0^t H(\xi)d\xi\right) dz\right) \cdot \exp\left(-\int_0^t H(\xi)d\xi\right) \geq 0, \tag{2.3}$$

where $S(0) \geq 0$ for all $t > 0$.

The other state variables are solved by the similar ways for $(I, Q, R)(0) \geq 0$. Therefore, the solutions of system (2.1) are $(I, Q, R)(t) > 0$ for every $t > 0$. □

Theorem 2 *Let* (S, I, Q, R) *be the solution of system* (2.1) *with the initial conditions* $(S, I, Q, R)(0)$. *Then*, $(S, I, Q, R)(t)$ *are bounded in a region* Ω.

Proof Let $N(t)$ be total population of system (2.1) stated as $N(t) = (S + I + Q + R)(t)$. Then, derivative in t, one has

$$\begin{aligned}\frac{dN}{dt} &= \frac{d(S + I + Q + R)}{dt} \\ &= \Lambda - \mu(S + I + Q + R)(t) - d(I + Q).\end{aligned}$$

At disease-free $d(I + Q) = 0$

$$\frac{dN}{dt} = \Lambda - \mu(S + I + Q + R)(t). \tag{2.4}$$

Due to $S + I + Q + R = N$,

$$\frac{dN}{dt} \leq \Lambda - \mu N(t),$$

Applying the integration for both sides, then one has

$$\begin{aligned}\int_{N(0)}^{N(t)} \frac{dN}{\Lambda - \mu N} &\leq \int_0^t dt, \\ N(t) &\leq N(0)e^{-\mu t} + \frac{\Lambda}{\mu}\left(1 - e^{-\mu t}\right)\end{aligned}$$

Hence

$$\lim_{t\to\infty} \sup N(t) \leq \frac{\Lambda}{\mu}.$$

Therefore, the bounded region of system (2.1) where it has biological and epidemiological meaningful can be stated as follows

$$\Omega = \left\{(S, I, Q, R)(t) \in \mathbb{R} : 0 \leq N(t) \leq \frac{\Lambda}{\mu}\right\}.$$

□

The existence and uniqueness of the solution of system (2.1) can be provided through the maximality condition which is stated in the following theorem.

Theorem 3 *Let* C_j, C_j^* *be the constant for* $j = 1, 2, 3, 4$ *such that*

$$\begin{aligned}&|\mathcal{F}_j(M_j, t) - \mathcal{F}_j(M_j^*, t)|^2 \leq C_j|M_j - M_j^*|^2, \\ &|\mathcal{F}_j(M_j, t)|^2 \leq C_j^*(1 + |M_j|^2), \text{ or } |\mathcal{F}_j(M_j, t)|^2 \leq C_j^*|M_j|^2,\end{aligned} \tag{2.5}$$

for all $(M, t) \in \mathbb{R} \times (0, T)$.

Proof We firstly give the notation of $\mathcal{F}_j, M_j$, and M_j^* for all state variables S, I, Q, R as follows

$$\begin{aligned}
\mathcal{F}_1(S,I,Q,R,t) &:= \frac{dS}{dt} = \Lambda - \beta\delta SI - \mu S,\\
\mathcal{F}_2(S,I,Q,R,t) &:= \frac{dI}{dt} = \beta\delta SI - (r+\epsilon+\mu+d)I,\\
\mathcal{F}_3(S,I,Q,R,t) &:= \frac{dQ}{dt} = \epsilon I - (\varphi+d+\mu)Q,\\
\mathcal{F}_4(S,I,Q,R,t) &:= \frac{dR}{dt} = rI + \varphi Q - \mu R,\\
(M_1,M_2,M_3,M_4) &:= (S,I,Q,R),\\
(M_1^*,M_2^*,M_3^*,M_4^*) &:= (S^*,I^*,Q^*,R^*).
\end{aligned} \tag{2.6}$$

It follows from (2.6) and first inequality of (2.5) for first state variable, one has

$$\begin{aligned}
|\mathcal{F}_1(S,t) - \mathcal{F}_1(S^*,t)|^2 &= |-\beta\delta(S-S^*)I - \mu(S-S^*)|^2\\
&\le 2|\beta\delta I + \mu|^2|S-S^*|^2\\
&\le 2\left(\beta^2\delta^2 \sup_{0\le t\le\tau}|I|^2 + \mu^2\right)|S-S^*|^2\\
&\le \mathcal{C}_1|S-S^*|^2,
\end{aligned} \tag{2.7}$$

where $\mathcal{C}_1 = 2\left(\beta^2\delta^2\|I\|_\infty^2 + \mu^2\right)$. Similarly for $|\mathcal{F}_2(I,t) - \mathcal{F}_2(I^*,t)|^2 \le \mathcal{C}_2|I-I^*|^2$, $|\mathcal{F}_3(Q,t) - \mathcal{F}_3(Q^*,t)|^2 \le \mathcal{C}_3|Q-Q^*|^2$, $|\mathcal{F}_4(R,t) - \mathcal{F}_4(R^*,t)|^2 \le \mathcal{C}_4|R-R^*|^2$, then one has

$$\begin{aligned}
|\mathcal{F}_2(I,t) - \mathcal{F}_2(I^*,t)|^2 &= |\beta\delta S - (r+\epsilon+\mu+d)(I-I^*)|^2\\
&\le 2|\beta\delta S - (r+\epsilon+\mu+d)|^2|I-I^*|^2\\
&\le 2\left(\beta^2\delta^2 \sup_{0\le t\le\tau}|S|^2 + (r^2+\epsilon^2+\mu^2+d^2)\right)|I-I^*|^2\\
&\le \mathcal{C}_2|I-I^*|^2,
\end{aligned} \tag{2.8}$$

$$\begin{aligned}
|\mathcal{F}_3(Q,t) - \mathcal{F}_3(Q^*,t)|^2 &= |-(\varphi+d+\mu)(Q-Q^*)|^2\\
&\le 2(\varphi^2+d^2+\mu^2)|Q-Q^*|^2\\
&\le \mathcal{C}_3|I-I^*|^2,
\end{aligned} \tag{2.9}$$

$$\begin{aligned}
|\mathcal{F}_4(R,t) - \mathcal{F}_4(R^*,t)|^2 &= |-\mu(R-R^*)|^2\\
&\le 2\mu^2|R-R^*|^2\\
&\le \mathcal{C}_4|R-R^*|^2,
\end{aligned} \tag{2.10}$$

where $\mathcal{C}_2 = 2\left(\beta^2\delta^2\|S\|_\infty^2 + (r^2+\epsilon^2+\mu^2+d^2)\right)$, $\mathcal{C}_3 = 2(\varphi^2+d^2+\mu^2)$, and $\mathcal{C}_4 = 2\mu^2$. Based on the results of (2.7)–(2.10), one proves the first inequality of (2.5). To prove the second inequality of (2.5), one has first state variable as follows

$$
\begin{aligned}
|\mathcal{F}_1(S,t)|^2 &= |\Lambda - \beta\delta SI - \mu S|^2 \\
&\leq 2\Lambda^2 + 2\left(\beta^2\delta^2 \sup_{0\leq t\leq\tau}|I|^2 + \mu^2\right)|S|^2 \\
&\leq 2\Lambda^2 + 2\left(\beta^2\delta^2\|I\|_\infty^2 + \mu^2\right)|S|^2 \\
&\leq \mathcal{C}_1^*(1+|S|^2),
\end{aligned}
\tag{2.11}
$$

which implies $\frac{\beta^2\delta^2\|I\|_\infty^2+\mu^2}{\Lambda^2} < 1$, where $\mathcal{C}_1^* = \Lambda^2$. Similarly, for second state variable, we have

$$
\begin{aligned}
|\mathcal{F}_2(I,t)|^2 &= |\beta\delta SI - (r+\epsilon+\mu+d)I|^2 \\
&\leq 2\left(\beta^2\delta^2 \sup_{0\leq t\leq\tau}|S|^2 + (r^2+\epsilon^2+\mu^2+d^2)\right)|I|^2 \\
&\leq \mathcal{C}_2^*|I|^2,
\end{aligned}
\tag{2.12}
$$

where $\mathcal{C}_2^* = \beta^2\delta^2\|S\|_\infty^2 + (r^2+\epsilon^2+\mu^2+d^2)$. For third state variables, one provides

$$
\begin{aligned}
|\mathcal{F}_3(Q,t)|^2 &= |\epsilon I - (\varphi+d+\mu)Q|^2 \\
&\leq 2\epsilon^2 \sup_{0\leq t\leq\tau}|I|^2 + 2(\varphi^2+d^2+\mu^2)|Q|^2 \\
&\leq 2\|I\|_\infty^2 + 2(\varphi^2+d^2+\mu^2)|Q|^2 \\
&\leq \mathcal{C}_3^*(1+|Q|^2),
\end{aligned}
\tag{2.13}
$$

which implies $\frac{\varphi^2+d^2+\mu^2}{\epsilon^2\|I\|_\infty^2} < 1$, where $\mathcal{C}_3^* = \epsilon^2\|I\|_\infty^2$. Finally, the fourth state variable gives

$$
\begin{aligned}
|\mathcal{F}_4(R,t)|^2 &= |rI + \varphi Q - \mu R|^2 \\
&\leq 2r^2 \sup_{0\leq t\leq\tau}|I|^2 + 2\varphi^2 \sup_{0\leq t\leq\tau}|Q|^2 + 2\mu^2|R|^2 \\
&\leq 2r^2\|I\|_\infty^2 + 2\varphi^2\|Q\|_\infty^2 + 2\mu^2|R|^2 \\
&\leq \mathcal{C}_4^*(1+|R|^2),
\end{aligned}
\tag{2.14}
$$

which implies $\frac{\mu^2}{r^2\|I\|_\infty^2+\varphi^2\|Q\|_\infty^2} < 1$, where $\mathcal{C}_4^* = r^2\|I\|_\infty^2 + \varphi^2\|Q\|_\infty^2$. Employing the following maximality condition

$$
Max\left\{\frac{\beta^2\delta^2\|I\|_\infty^2+\mu^2}{\Lambda^2}, \frac{\varphi^2+d^2+\mu^2}{\epsilon^2\|I\|_\infty^2}, \frac{\mu^2}{r^2\|I\|_\infty^2+\varphi^2\|Q\|_\infty^2}\right\} < 1.
$$

Then the second conditions of (2.5) can be provided. □

Stability Analysis

Equilibria and the Basic Reproduction Number

This section provides the equilibria points and reproduction number $\mathcal{R}_0$. In epidemiology, the basic reproduction number $\mathcal{R}_0$ of an infection can be thought of as the number of cases produced by one case, on average during its infectious period, in an uninfected

population [27]. This basic reproduction number is helpful to ensure that infectious disease can transmit or not in the population. If $\mathcal{R}_0 < 1$ the infection will stop in the long term. Moreover, if $\mathcal{R}_0 > 1$ the infection has the ability to transmit in the population. In general, if the $\mathcal{R}_0$ value is greater, then the control of epidemic is more difficult.

Theorem 4 *In system* (2.1), *there is a disease-free equilibrium when the basic reproduction number* $\mathcal{R}_0 < 1$, *i.e.*,

$$E^0 = (S^0, I^0, Q^0, R^0) = \left(\frac{\Lambda}{\mu}, 0, 0, 0\right). \tag{3.1}$$

Moreover, *there is an endemic disease equilibrium when the basic reproduction number* $\mathcal{R}_0 > 1$, *i.e.*,

$$E^* = (S^*, I^*, Q^*, R^*), \tag{3.2}$$

where

$$S^* = \frac{r+\epsilon+\mu+d}{\beta\delta},\ I^* = \frac{\Lambda}{r+\epsilon+\mu+d} - \frac{\mu}{\beta\delta},$$
$$Q^* = \frac{\epsilon}{\varphi+d+\mu} I^*,\ R^* = \frac{r}{\mu} I^* + \frac{\varphi}{\mu} Q^*.$$

Proof By considering the derivatives in the left-hand side of system (2.1) equal to zero and $I = 0$, then one has a disease-free equilibrium E^0. Moreover, applying $I \neq 0$, we can get an endemic disease equilibrium E^*. □

The next generation matrix is then used to get the basic reproduction number R_0 of (2.1). By linearizing around the disease-free equilibrium (E^0), one has

$$\begin{aligned}\begin{pmatrix} I \\ Q \end{pmatrix}_t &= \begin{pmatrix} \beta\delta SI - (r+\epsilon+\mu+d)I \\ \epsilon I - (\varphi+d+\mu)Q \end{pmatrix} \\ &= \left[\begin{pmatrix} \beta\delta S & 0 \\ 0 & 0 \end{pmatrix} - \begin{pmatrix} r+\epsilon+\mu+d & 0 \\ epsilon & \varphi+d+\mu \end{pmatrix}\right] \begin{pmatrix} I \\ Q \end{pmatrix} \\ &= (\mathcal{F} - \mathcal{V}) \begin{pmatrix} I \\ Q \end{pmatrix},\end{aligned}$$

where $\mathcal{F}$ is the transmission matrix of new infected individuals, and $\mathcal{V}$ is the transition matrix of individual displacements between groups of individuals. Then, the next generation matrix can be expressed as

$$\mathcal{F}\mathcal{V}^{-1} = \begin{pmatrix} \frac{\Lambda\beta\delta}{\mu(r+\epsilon+\mu+d)} & 0 \\ 0 & 0 \end{pmatrix}$$

Therefore, based on the dominant eigenvalues of next generation matrix, one has the basic reproduction number

$$\mathcal{R}_0 = \frac{\Lambda\beta\delta}{\mu(r+\epsilon+\mu+d)}. \tag{3.3}$$

Local Stability of the Disease-Free Equilibrium

Theorem 5 *The disease-free equilibrium E^0 is local asymptotically stable if $\mathcal{R}_0 < 1$.*

Proof We firstly provide the Jacobian matrix of system (2.1) at the disease-free equilibrium E^0 as follows

$$J(E^0) = \begin{pmatrix} -\mu & -\frac{\Lambda\beta\delta}{\mu} & 0 & 0 \\ 0 & \frac{\Lambda\beta\delta}{\mu} - (r+\epsilon+\mu+d) & 0 & 0 \\ 0 & \epsilon & -(\varphi+d+\mu) & 0 \\ 0 & r & \varphi & -\mu \end{pmatrix}. \tag{3.4}$$

The eigenvalues of (3.4) are easy to obtain by solving the characteristic equation $|J(E^0) - \lambda I_d| = 0$, then one has

$$\begin{aligned} &\lambda_1 = -\mu < 0,\ \lambda_2 = -(\varphi+d+\mu) < 0, \\ &\lambda_3 = \frac{-\left(\frac{\Lambda\beta\delta}{\mu} - (r+\epsilon+\mu+d)\right) - \sqrt{\mathcal{D}}}{2} \\ &\lambda_4 = \frac{-\left(\frac{\Lambda\beta\delta}{\mu} - (r+\epsilon+\mu+d)\right) + \sqrt{\mathcal{D}}}{2}, \end{aligned} \tag{3.5}$$

where

$$\mathcal{D} = \left(\frac{\Lambda\beta\delta}{\mu} - (r+\epsilon+\mu+d)\right)^2 - 4\mu(r+\epsilon+\mu+d) + 4\Lambda\beta\delta > 0.$$

Therefore, λ_3 is negative. If $R_0 < 1$, then one has $\Lambda\beta\delta < \mu(r+\epsilon+\mu+d)$, implying that

$$\mathcal{D} < \left(\frac{\Lambda\beta\delta}{\mu} - (r+\epsilon+\mu+d)\right)^2.$$

Then

$$\lambda_4 < \frac{-\left(\frac{\Lambda\beta\delta}{\mu} - (r+\epsilon+\mu+d)\right) + \sqrt{\left(\frac{\Lambda\beta\delta}{\mu} - (r+\epsilon+\mu+d)\right)^2}}{2} = 0.$$

Because all eigenvalues $\lambda_i < 0$ for $i = 1, 2, 3, 4$, we can conclude that the equilibrium E^0 is local asymptotically stable. □

Figure 1 shows the function of R_0 with the independent variables β and ϵ. It is clear that R_0 increases as infection rate β increases and R_0 decreases as isolation rate ϵ increases. The most effective to control the CoVid-19 spread is to control reproduction number R_0 less than one. Based on this principle, the strategy of isolation should be advocated, so the viruses spread will be decreased.

Local Stability of the Endemic Disease Equilibrium

Theorem 6 *The endemic disease equilibrium E^* is local asymptotically stable if $\mathcal{R}_0 > 1$.*

Proof Similarly, we firstly provide the Jacobian matrix of system (2.1) at the endemic disease equilibrium E^* as follows

$$J(E^*) = \begin{pmatrix} -\beta\delta I^* - \mu & -\beta\delta S^* & 0 & 0 \\ \beta\delta I^* & \beta\delta S^* - (r+\epsilon+\mu+d) & 0 & 0 \\ 0 & \epsilon & -(\varphi+d+\mu) & 0 \\ 0 & r & \varphi & -\mu \end{pmatrix}. \tag{3.6}$$

The eigenvalues of (3.4) are similar ways as in Theorem 5 to obtain by solving the characteristic equation $|J(E^*) - \lambda I_d| = 0$. We determine the minor values of $J(E^*)$ to get the cofactor expansion, then the eigenvalues satisfy the following equation

$$(-\mu - \lambda)(-(\varphi + d + \mu) - \lambda)\det(A) = 0, \tag{3.7}$$

where

$$A = \begin{pmatrix} -\beta\delta I^* - \mu & -\beta\delta S^* \\ \beta\delta I^* & \beta\delta S^* - (r+\epsilon+\mu+d) \end{pmatrix}. \tag{3.8}$$

Obviously, $\lambda_1 = -\mu < 0$, $\lambda_2 = -(\varphi + d + \mu) < 0$. Moreover, the eigenvalues $\lambda_{3,4}$ provide the stability criterion. All eigenvalues of the matrix A will be real and negative if

$$Tr(A) = \lambda_3 + \lambda_4 < 0,\ Det(A) = \lambda_3 \cdot \lambda_4 > 0.$$

Using the matrix A, one has

$$Tr(A) = -\frac{\Lambda\beta\delta}{r+\epsilon+\mu+d} < 0$$
$$Det(A) = \mu(\mathcal{R}_0 - 1)(r+\epsilon+\mu+d).$$

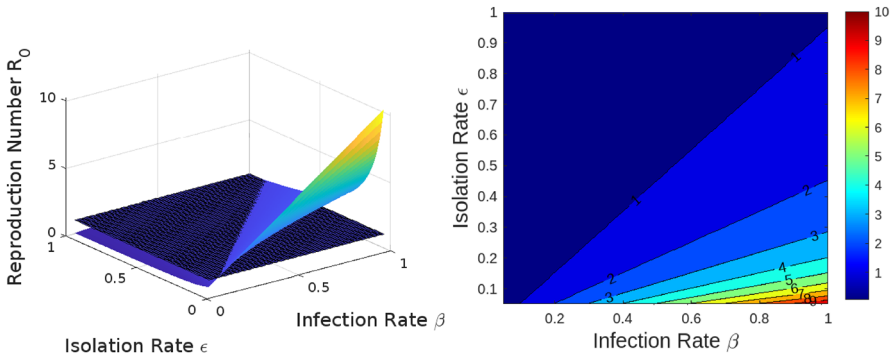

Fig. 1 Tendency of R_0 with infection rate β and isolation rate ϵ

Based on the above results, all eigenvalues of matrix (3.8) are negative real part if $R_0 > 1$. Thus, the equilibrium E^* is local asymptotically stable. □

Global Stability of the Disease-Free Equilibrium

To establish the global stability at the disease-free equilibrium E_0, there are two conditions that must be satisfied [16]. Initially, the Eq. (2.1) is divided into two systems as follows

$$\begin{aligned} \frac{dY_1}{dt} &= F_1(Y_1, Y_2), \\ \frac{dY_2}{dt} &= F_2(Y_1, Y_2),\ F_2(Y_1, 0) = 0, \end{aligned} \tag{3.9}$$

where $Y_1 = (S, R)$ provides the number of uninfected individuals and $Y_2 = (I, Q)$ provides the number of infected individuals. Moreover, $\mathcal{P}_0 = (Y_1^0, 0)$ denotes the disease-free equilibrium of the Eq. (3.9). It follows from Eq. (3.1) and Eq. (3.9), one has $\mathcal{P}_0 = (Y_1^0, 0) = (S^0, 0)$. Then, the following two conditions must be satisfied to guarantee the global asymptotically stability.

(H1) If $\dfrac{dY_1}{dt} = F_1(Y_1, 0)$, then Y_1^0 is global asymptotically stable,

(H2) If $(Y_1, Y_2) \in \Omega$, then $F_2(Y_1, Y_2) = \mathcal{M}Y_2 - \mathcal{K}(Y_1, Y_2)$ for $\mathcal{K}(Y_1, Y_2) \geq 0$,

where

$$\mathcal{M} = \frac{dF_2}{dY_2}(Y_1^0, 0).$$

Theorem 7 *Let $\mathcal{P}_0 = (Y_1^*, 0)$ be disease-free equilibrium of Eq. (3.9). Then the fixed point $\mathcal{P}_0$ is global asymptotically stable in the interior Ω if $\mathcal{R}_0 < 1$ and the conditions (H1) and (H2) are satisfied.*

Proof Since $\frac{dY_1}{dt} = F_1(Y_1, 0)$ gives

$$\begin{aligned} \frac{dS}{dt} &= \Lambda - \mu S, \\ \frac{dR}{dt} &= -\mu R. \end{aligned}$$

Then, by conducting the limit $t \to +\infty$, one has

$$(S, R) \to \left(\frac{\Lambda}{\mu}, 0\right) = (Y_1^0, 0),$$

implying that $(S, R) \to (S^0, 0)$ and Y_1^0 is global asymptotically stable. Since $Y_1 = (S, R)$, $Y_2 = (I, Q)$ and the assumption $S \sim N$ at the early phase of epidemic, then one can establish

$$F_1(Y_1, 0) = \left(\frac{\Lambda}{\mu}, 0\right),$$
$$\mathcal{M} = \begin{pmatrix} \beta\delta N - (r + \epsilon + \mu + d) & 0 \\ \epsilon & -(\varphi + d + \mu) \end{pmatrix},$$
$$\mathcal{K}(Y_1, Y_2) = \begin{pmatrix} \beta\delta I(N - S) \\ 0 \end{pmatrix}.$$

It follows from Eq. (2.6) and $N = S + I + Q + R$ then one has $0 \leq S \leq N$, implying that $\mathcal{K}(Y_1, Y_2) \geq 0$. If the matrix $\mathcal{M}$ is irreducible and $\mathcal{K}(Y_1, Y_2) \geq 0$ then the theorem becomes true for $\mathcal{R}_0 < 1$. Hence, the fixed point $\mathcal{P}_0 = (Y_1^*, 0)$ is global asymptotically stable in the interior Ω. □

Global Stability of the Endemic Disease Equilibrium

Theorem 8 *The endemic disease equilibrium E^* is global asymptotically stable on the interior Ω if $\mathcal{R}_0 > 1$.*

Proof Let the Lyapunov function $\mathcal{L}$ be defined as

$$\mathcal{L}(x_i) = \sum_{i=1}^{N} \frac{1}{2}(x_i - x_i^*)^2, \tag{3.10}$$

where

N = number of state variables (S, I, Q, R),
$x_i = i^{th}$ state variable,
$x_i^* = i^{th}$ state variable for endemic disease equilibrium.

Applying (3.10) into the system of (2.1), then one has

$$\mathcal{L}(S, I, Q, R) = \frac{1}{2}[(S - S^*) + (I - I^*) + (Q - Q^*) + (R - R^*)]^2.$$

Differentiating the above results with respect to t, one further has

$$\frac{d\mathcal{L}}{dt} = [(S - S^*) + (I - I^*) + (Q - Q^*) + (R - R^*)]\frac{d}{dt}(S + I + Q + R). \tag{3.11}$$

Based on (2.4), one gets

$$N^* = (S^* + I^* + Q^* + R^*) = \frac{\Lambda}{\mu}. \tag{3.12}$$

Substituting (2.4) and (3.12) into (3.11) gives

$$\begin{aligned}\frac{d\mathcal{L}}{dt} &= \left[N - \frac{\Lambda}{\mu}\right][\Lambda - N\mu] \\ &= \left[2N\Lambda - N^2\mu - \frac{\Lambda^2}{\mu}\right] \\ &= -\frac{1}{\mu}\left[\Lambda^2 - 2N\Lambda\mu + N^2\mu^2\right] \\ &= -\frac{1}{\mu}[\Lambda - N\mu]^2 < 0.\end{aligned} \tag{3.13}$$

Then $\frac{d\mathcal{L}}{dt}$ is a Lyapunov function as stated in (3.13), which concludes that the endemic disease equilibrium E^* is global asymptotically stable. □

Optimal Control

In this section, the mathematical model of CoVid-19 with the control of vaccination and social distancing is formulated. Based on the sensitivity index of lockdown (δ), this paremeter gives the significant impact for the basic reproduction number with the sensitivity index $\Gamma_{\delta}^{\mathcal{R}_0} = 100\%$. The significant impact of lockdown becomes a reason to consider the optimal control of this parameter. Moreover, the control of the transmission rate will give a good impact of reducing the spread of CoVid-19 in the community. Therefore, we provide the control of social distancing (u_2) and vaccination (u_1) to degrade the CoVid-19 transmission in the population. The mathematical model of CoVid-19 with the presence of control can be stated as follows

$$\begin{aligned}\frac{dS}{dt} &= (1-u_1)\Lambda - (1-u_2)\beta\delta SI - \mu S, \\ \frac{dI}{dt} &= (1-u_2)\beta\delta SI - (r+\epsilon+\mu+d)I, \\ \frac{dQ}{dt} &= \epsilon I - (\varphi+d+\mu)Q, \\ \frac{dR}{dt} &= u_1\Lambda + rI + \varphi Q - \mu R.\end{aligned} \tag{4.1}$$

The aim of the objective function is to minimize the CoVid-19 transmission by introducing two controls of vaccination (u_1) and social distancing (u_2), and also to minimize the control costs. Therefore, the objective function of system (4.1) is given below

$$\mathcal{J}(u_1, u_2) := \min \int_0^T \left[I(t) + \frac{A_1}{2}u_1^2(t) + \frac{A_2}{2}u_2^2(t)\right]dt, \tag{4.2}$$

where A_1 and A_2 are the cost factors with respect to controls u_1 and u_2, and T is final time of control implementations.

Pontryagin's maximum principle establishes the necessary conditions that the quadratic objective function must satisfy. This principle has the role to convert the system (4.1) and the objective functional $\mathcal{J}$ (4.2) into the minimizing pointwise problem known as the Hamiltonian

$\mathcal{H}$ with respect to controls $(u_1, u_2)(t)$ for all $t \in [0, T]$. The Hamiltonian referring to the system (4.1) and quadratic objective functional (4.2) can be formulated as follows

$$\begin{aligned}\mathcal{H} = I + \frac{A_1}{2}u_1^2(t) + \frac{A_2}{2}u_2^2(t) + \psi_1\big[(1-u_1)\Lambda - (1-u_2)\beta\delta SI - \mu\big] \\ + \psi_2\big[(1-u_2)\beta\delta SI - (r+\epsilon+\mu+d)I\big] + \psi_3[\epsilon I - (\varphi+d+\mu)Q] \\ + \psi_4\big[u_1\Lambda + \varphi Q - \mu R\big],\end{aligned} \tag{4.3}$$

where ψ_i for $i = 1, 2, 3, 4$ are the adjoint variables for each state variable S, I, Q, R respectively. Let $\mathcal{U}$ be a non-empty control set stated as follows

$$\mathcal{U} := \big\{(u_1, u_2) : u_i \text{ is Lebesgue measurable}, u_i \in [0, 1] \text{ for } i = 1, 2, t \in [0, T]\big\}. \tag{4.4}$$

Then, the optimal control $u^* = (u_1^*, u_2^*)$ is defined as follows

$$\mathcal{J}(u^*) := \min\big\{\mathcal{J}(u_1, u_2) : u_1, u_2 \in \mathcal{U}\big\}. \tag{4.5}$$

Theorem 9 *Let $u^* = (u_i^*)$ for $i = 1, 2$ be an optimal control and S^*, I^*, Q^*, R^* be the solutions of system (4.1) minimizing $\mathcal{J}(u^*)$ over the control set $\mathcal{U}$ defined in (4.4), then there exists adjoint variables ψ_i for $i = 1, 2, 3, 4$ satisfying*

$$\begin{aligned}\frac{d\psi_1}{dt} &= \mu\psi_1 + (1-u_2)\beta\delta I^*, \\ \frac{d\psi_2}{dt} &= (1-u_2)(\psi_1 - \psi_2)\beta\delta S + (r+\epsilon+\mu+d)\psi_2 - \epsilon\psi_3 - r\psi_4, \\ \frac{d\psi_3}{dt} &= \psi_3(\varphi+d+\mu) - \psi_4\varphi, \\ \frac{d\psi_4}{dt} &= \psi_4\mu.\end{aligned} \tag{4.6}$$

with transversality conditions $\psi_i(T) = 0$, for $i = 1, 2, 3, 4$, and

$$u^* = \begin{cases} u_1^*(t) = \min\left\{\max\left\{0, \frac{\Lambda(\psi_1-\psi_4)}{A_1}\right\}, u_{1_{\max}}\right\}, \\ u_2^*(t) = \min\left\{\max\left\{0, \frac{\beta\delta SI(\psi_2-\psi_1)}{A_2}\right\}, u_{2_{\max}}\right\}. \end{cases} \tag{4.7}$$

Proof Pontryagin et al. [41] provides the adjoint system and transversality conditions with respect to this optimal control. For this purpose, we establish the derivative of Hamiltonian function (4.3) with respect to S, I, Q, R as stated as follows

$$\begin{cases} \frac{d\psi_1}{dt} = -\frac{\partial\mathcal{H}}{\partial S}, & \psi_1(T) = 0, \\ \frac{d\psi_2}{dt} = -\frac{\partial\mathcal{H}}{\partial I}, & \psi_2(T) = 0, \\ \frac{d\psi_3}{dt} = -\frac{\partial\mathcal{H}}{\partial Q}, & \psi_3(T) = 0, \\ \frac{d\psi_4}{dt} = -\frac{\partial\mathcal{H}}{\partial R}, & \psi_4(T) = 0. \end{cases}$$

Meanwhile, the optimal control can be provided by finding the optimal solution of

Table 1 Parameter values and sensitivity index

Parameter	Description	Value	Sensitivity index
Λ	The birth rate	0.01	1
β	The transmission rate	0.01	1
δ	The lockdown	1	1
μ	The natural death rate	0.00003	−1
r	The cure rate related to infected	0.03	−0.4410
ϵ	The isolation rate	0.03	−0.4410
d	The disease-related death rate	0.008	−0.1176
φ	The cure rate related to isolation	0.04	–

$$\frac{\partial \mathcal{H}}{\partial u_i} = 0, \text{ for } u_i^* \text{ where } i = 1, 2.$$

We further apply the standard ways of bounds on the optimal control as written as follows

$$u_i^* = \begin{cases} 0 & \text{if } \phi_i^* \leq 0, \\ \phi_i^* & \text{if } 0 \leq \phi_i^* \leq u_{i_{\max}}, \\ u_{i_{\max}} & \text{if } \phi_i^* \geq u_{i_{\max}}, \end{cases}$$

where $i = 1, 2$ and

$$\phi_1^* = \frac{\Lambda(\psi_1 - \psi_4)}{A_1},$$
$$\phi_2^* = \frac{\beta\delta SI(\psi_2 - \psi_1)}{A_2}.$$

□

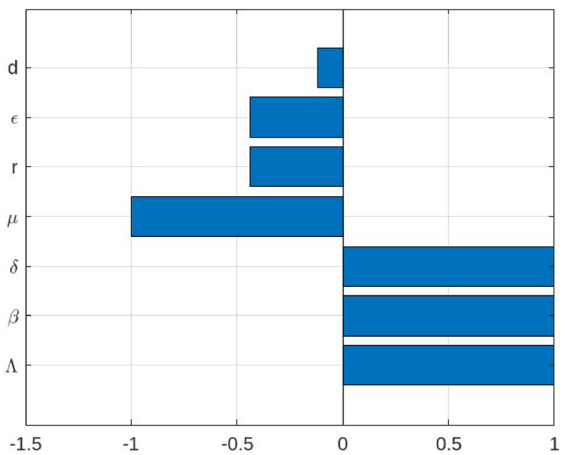

Fig. 2 PRCC results for $\mathcal{R}_0$

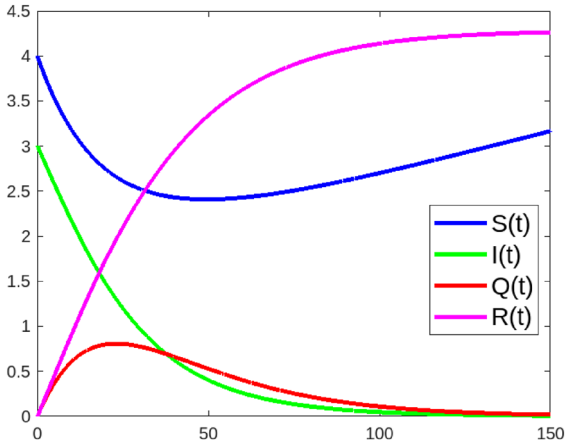

Fig. 3 Simulation of *SIQR* model

Numerical Results and Discussion

The first-order derivative differential equations of system (2.1) is solved numerically using the fourth order Runge-Kutta method. The sensitivity analysis of R_0 is then provided by applying the Partial Rank Correlation Coefficient (PRCC) method. The MATLAB codes are available in GitHub through this link: https://github.com/mghaniunair/SIQR-Model-on-CoVid-19.

Sensitivity Analysis

The effect of each parameters on the endemic treshold is provided in the sensitivity analysis. This essential method of sensitivity analysis shows the strength of each parameters of *SIQR* model [14]. Moreover, the parameter values are all assumed and presented in Table 1. Meanwhile, the sensitivity index of $\mathcal{R}_0$ depending differentiably on a parameter π can be stated as

$$\Gamma_{\pi}^{\mathcal{R}_0} = \frac{\partial \mathcal{R}_0}{\partial \pi} \times \frac{\pi}{\mathcal{R}_0}. \tag{5.1}$$

From (5.1), the sensitivity indices are calculated and provided in Table 1.

The parameters of birth rate Λ, transmission rate β, and lockdown δ achieve the most positive sensitivity index with the basic reproduction number $\Gamma_{\Lambda}^{\mathcal{R}_0} = \Gamma_{\beta}^{\mathcal{R}_0} = \Gamma_{\delta}^{\mathcal{R}_0} = 1$, which means that the greater the numbers of births, transmission, and lockdown in a susceptible population, the greater the chance of the number of infected individuals if there is direct contact. Moreover, the most negative sensitivity index is achieved by the natural death rate μ with the basic reproduction number $\Gamma_{\mu}^{\mathcal{R}_0} = -1$, which means that 100% of natural death rate plays an important role to reduce the transmission of disease. The transmission rate β and lockdown δ have the positive impact 100% for the basic reproduction number. This means that the lockdown have a significant impact on basic reproduction number. Moreover the isolation rate ϵ and cure rate related to infected r give the same impact of 44.10% to

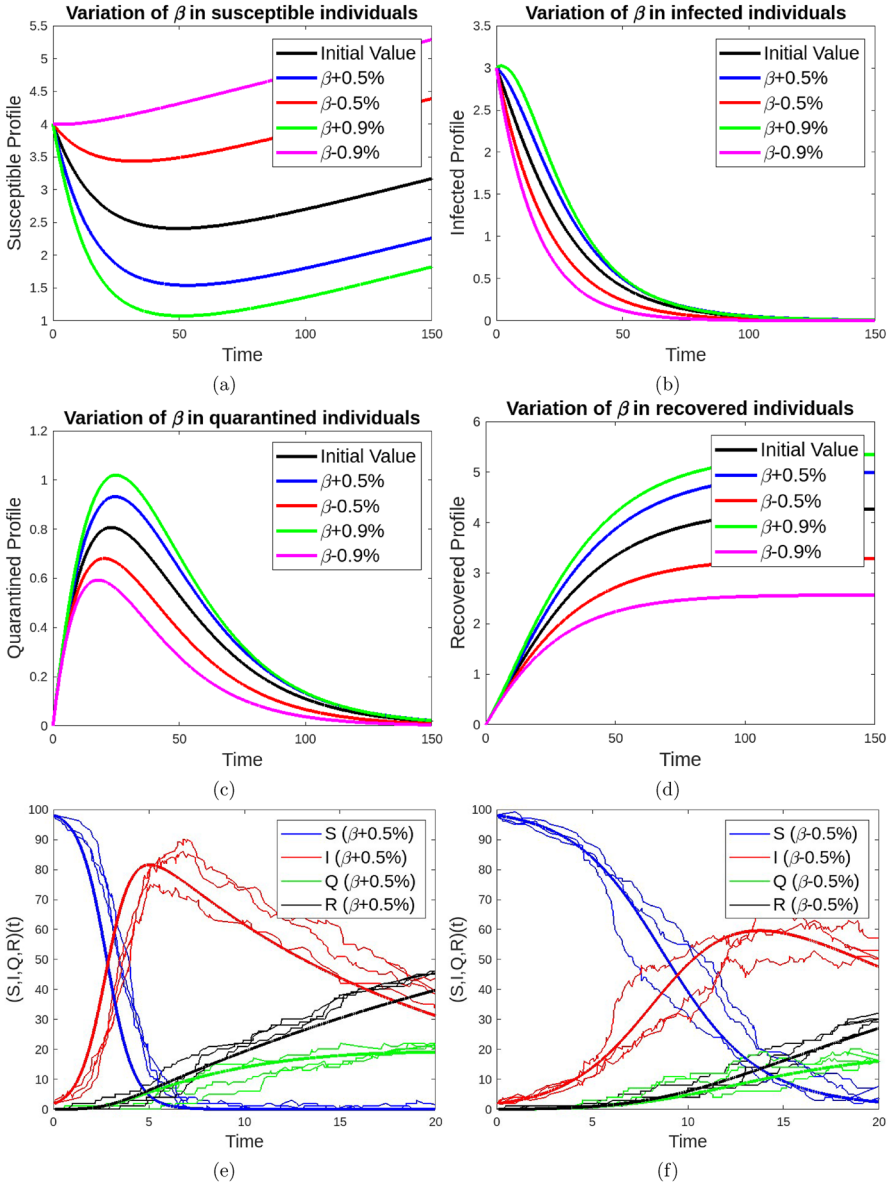

Fig. 4 Variation of β and deterministic versus stochastic in $(S, I, Q, R)(t)$

reduce (due to the negative sign as in Table 1) the number of disease transmission. Figure 2 provides the sensitivity analysis for 7 parameters of basic reproduction number $\mathcal{R}_0$. By referring to Eq. (3.3), there is no parameter of cure rate related to isolation φ for the basic reproduction number, which means that there is no significant impact for sensitivity index.

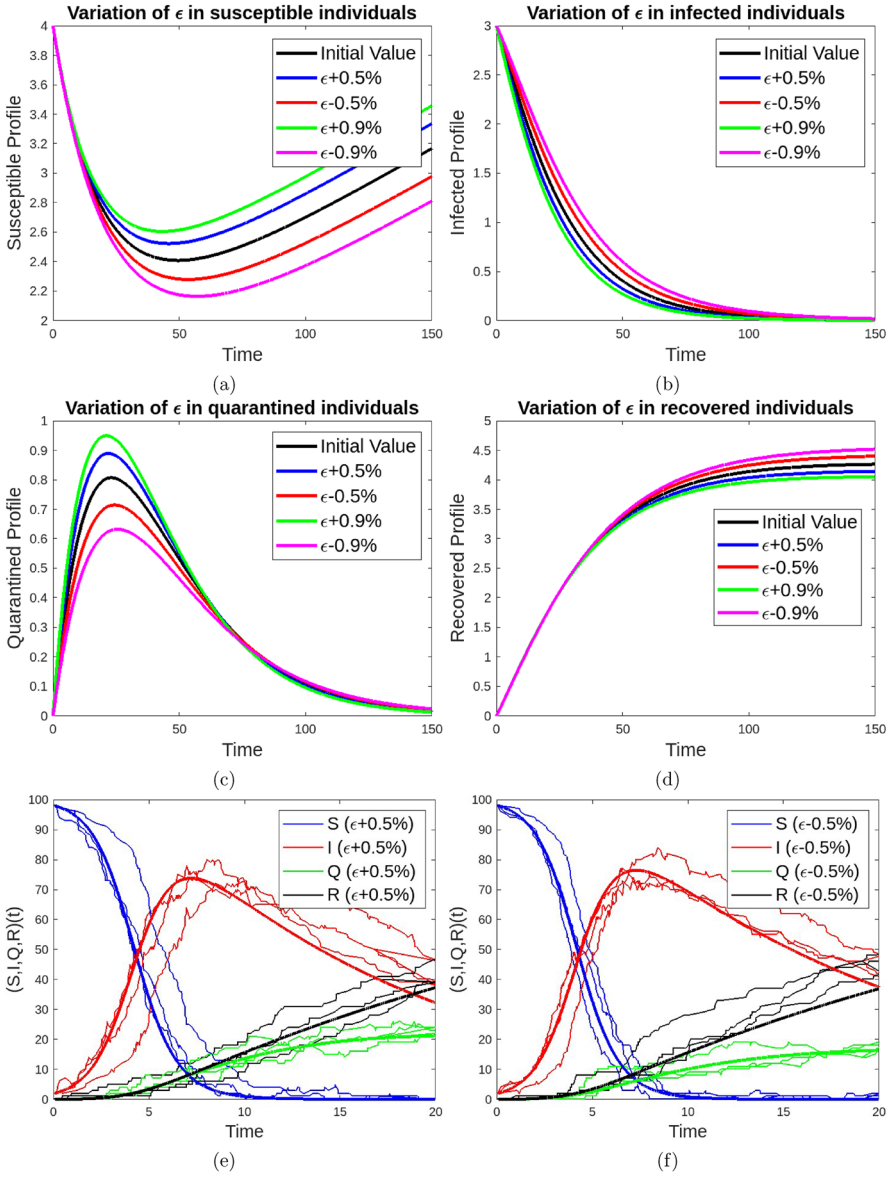

Fig. 5 Variation of ϵ and deterministic versus stochastic in $(S, I, Q, R)(t)$

Simulation of *SIQR* Model

The numerical simulation of our dynamical system (2.1) is provided in Fig. 3, which gives the descriptions that the susceptible class decreases due to the lockdown and at a time increases to reach the equilibrium point as the susceptible individuals move to the infected class and other individuals die naturally. Moreover, the infected class decreases as the individuals move from susceptible class to infected class, this may be caused by the isolation

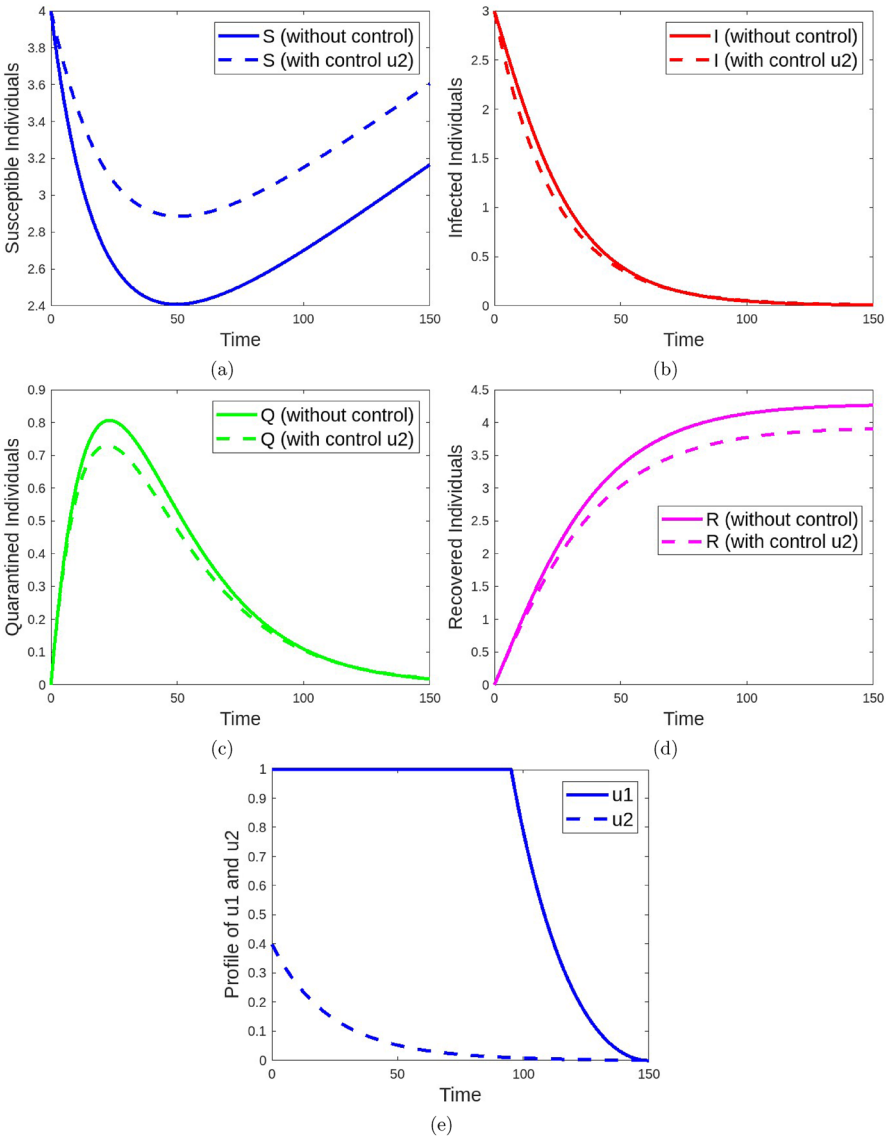

Fig. 6 Simulation of $SIQR(t)$ model with only optimal control $u_2(t)$, and profile of control $u_1(t)$ and $u_2(t)$

rate increasing the cure rate related to infected individuals and other impact is caused by the natural death. The quarantined class increases from the infected class and at a time decreases due to the individuals moving to recovered class to achieve the equilibrium point. The recovered class increases from susceptible, infected, and quarantined individuals due to the isolation rate, lockdown, and other individuals die naturally. The variables S, I, Q, R vary with time (t).

In the susceptible class as in Fig. 4, the decaying rate increases when the variation of transmission rate β increases. The susceptible individuals then move to the infected class,

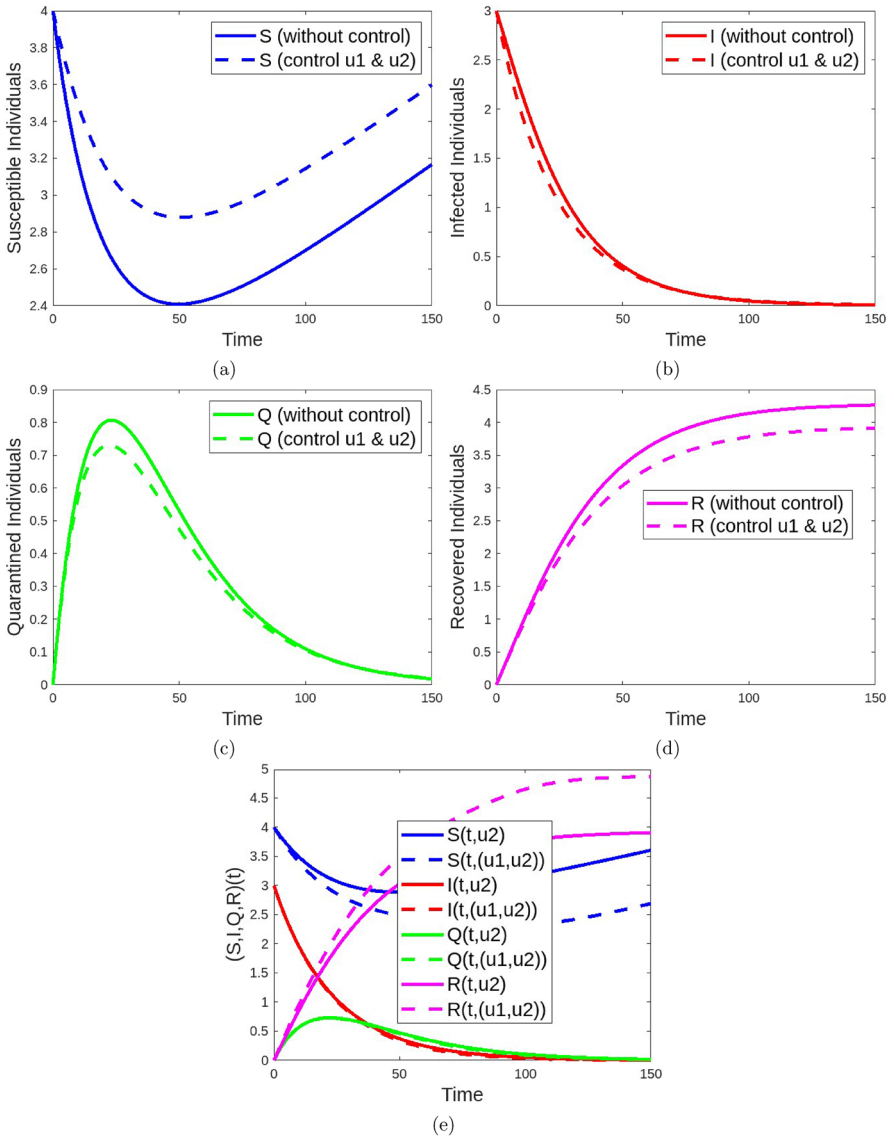

Fig. 7 Simulation of $SIQR(t)$ model with two optimal control $u_1(t)$ and $u_2(t)$

where this class provides the decreased decaying rate while the transmission rate increases (it also indicates the contact rate between susceptible and infected individuals). The infected class increases when the transmission rate increases and decreases by the individuals moving to quarantined class and isolation rate increases as in Fig. 4a, b. As shown in Fig. 4c, d, the quarantined class gives the similar results of decaying rate as in infected class which decrease when the transmission rate increases. The quarantined class will be increased when the transmission rate increases and will be decreased due to the individuals moving to recovered class and transmission rate decreasing. In this case, the number of recovered class will be increased because of individuals movement from quarantined class.

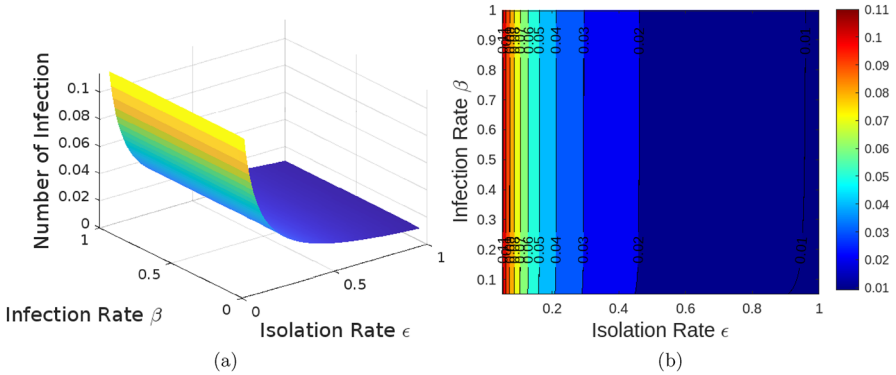

Fig. 8 Tendency of number of infection with infection rate β and isolation rate ϵ

Figure 5a provides that the decaying rate decreases when the variation of isolation rate increases. The susceptible individuals then move to the infected class. This infected class provides the increased decaying rate while the isolation rate increases as in Fig. 5b. The quarantined class will be decreased when the isolation rate increases and the individuals move to the quarantined class. Meanwhile, Fig. 5c shows the decreased decaying rate when the isolation rate increases which means that the quarantined individuals will be increased when isolation rate increases and will be decreased when the individuals move to the recovered class and die naturally. The individuals movement from quarantined class can affect the recovered individuals increased. For more detailed visualization of infected class, Fig. 8 gives the indication that the higher the isolation rate is the smaller the number of infection is and otherwise (from the contour, the red color indicates the higher number of infection than the other regions).

The simulation of $(S, I, Q, R)(t)$ model with optimal control $(u_1, u_2)(t)$ is based on the Eqs. (4.1), (4.6) and (4.7) by using the iterative method of fourth order Runge-Kutta with the assumptions of cost factors $A_1 = A_2 = 1$. As in Fig. 6a–d and Fig. 7a–d, there is a profile change for state variable $(S, I, Q, R)(t)$ without or with control $(u_1, u_2)(t)$ or only $u_2(t)$. The susceptible class with control $((u_1, u_2)(t)$ or only $u_2(t))$ gives the higher values than without control which means that the controls of only social distancing or the combinations between social distancing and vaccination provide the number of susceptible individuals increased. Meanwhile, the infected and quarantined classes are more decreased with control $((u_1, u_2)(t)$ or only $u_2(t))$ than without control. The results of infected class give the impact on the quarantined class, which means that if the infected individuals are decreased then automatically the quarantined individuals are also decreased. Moreover, the recovered class is more decreased with control $((u_1, u_2)(t)$ or only $u_2(t))$ than without control. This indicates that the vaccination and social distancing employed earlier in susceptible class (subject to Eq. (4.1)) give the significant impact for the susceptible, and infected classes, which means that the controls of vaccination and social distancing are not effective in recovered class. The profiles of two controls $(u_1, u_2)(t)$ and of $(S, I, Q, R)(t)$ with $(u_1, u_2)(t)$ or only $u_2(t)$ are provided in Fig. 6e and Fig. 7e respectively. As in Fig. 7e, it gives the results that there are significant difference between $(u_1, u_2)(t)$ and only $u_2(t)$ for each state variable $(S, I, Q, R)(t)$. The profile of recovered class with the combination of two controls (u_1, u_2) is greater than the profile of recovered class only with one control u_2. The

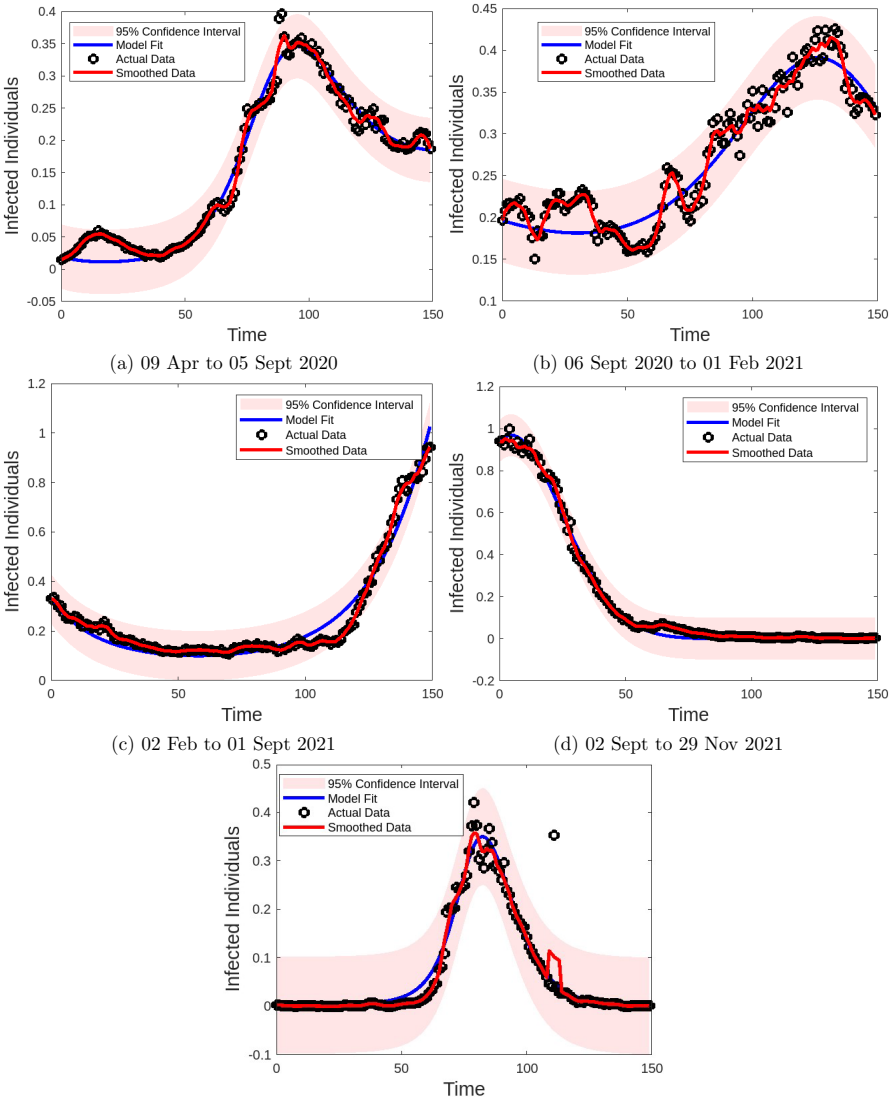

(a) 09 Apr to 05 Sept 2020

(b) 06 Sept 2020 to 01 Feb 2021

(c) 02 Feb to 01 Sept 2021

(d) 02 Sept to 29 Nov 2021

(e) 30 Nov 2021 to 16 May 2022

Fig. 9 Parameter fitting results of our *SIQR* model on CoVid-19 disease in Semarang, Indonesia (https://siagacorona.semarangkota.go.id/halaman/covid19pertahun/2020)

profiles of infected and quarantined class provide the same results, those two classes with the combination of two controls (u_1, u_2) are smaller than the ones only with one control u_2. Based on these results of infected, quarantined, and recovered classes, the susceptible class with the combination of two controls (u_1, u_2) are smaller than the ones only with one control u_2.

Fig. 10 Box-plot for all parameters $(\lambda, \beta, \delta, \mu, r, \epsilon, d, \varphi)$ with the range (09 Apr to 05 Sept 2020) and (06 ▶ Sept 2020 to 01 Feb 2021)

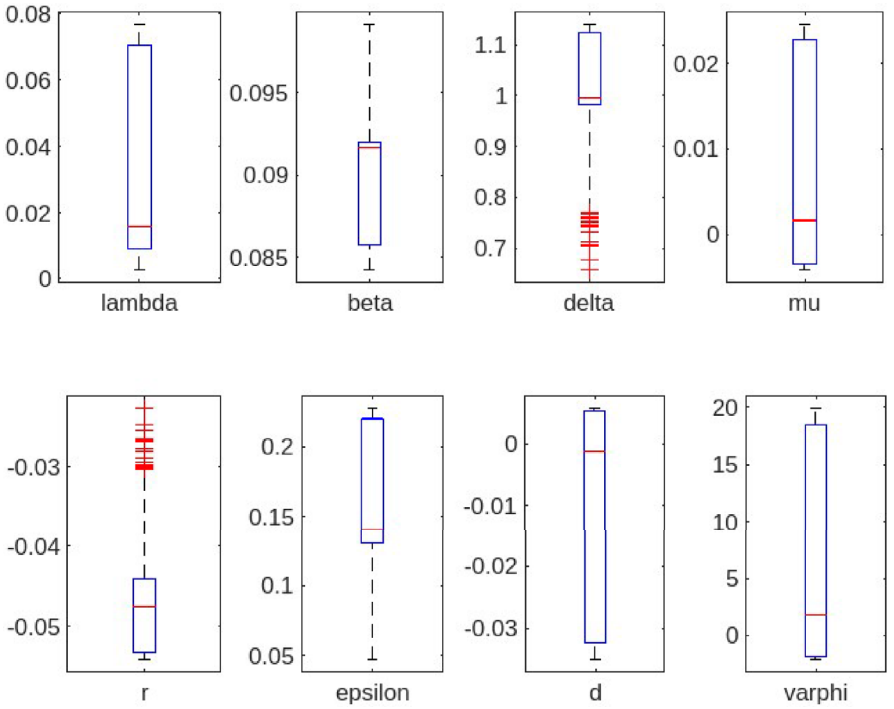

(a) 09 Apr to 05 Sept 2020

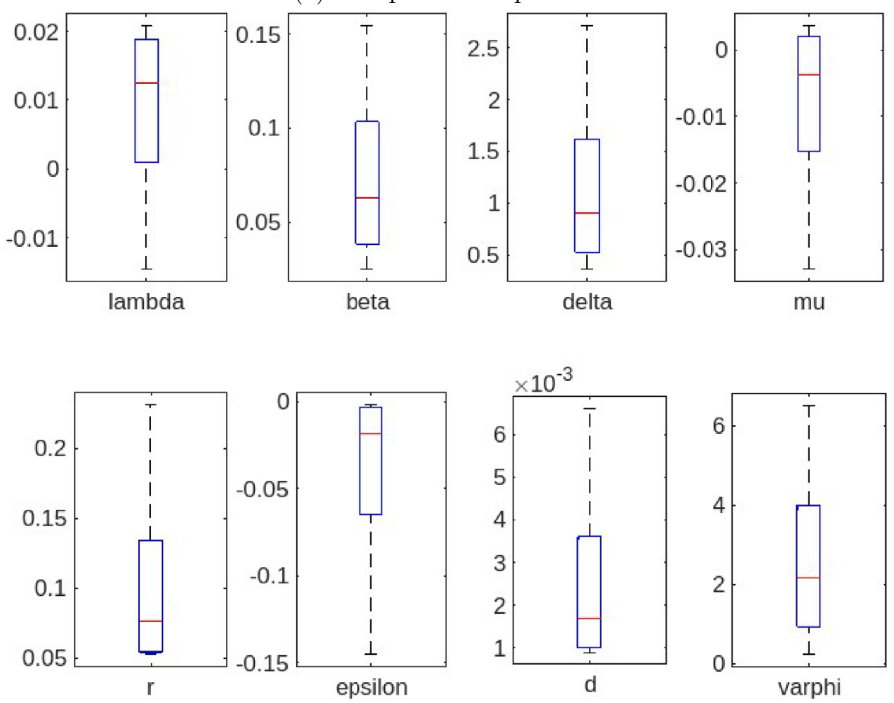

(b) 06 Sept 2020 to 01 Feb 2021

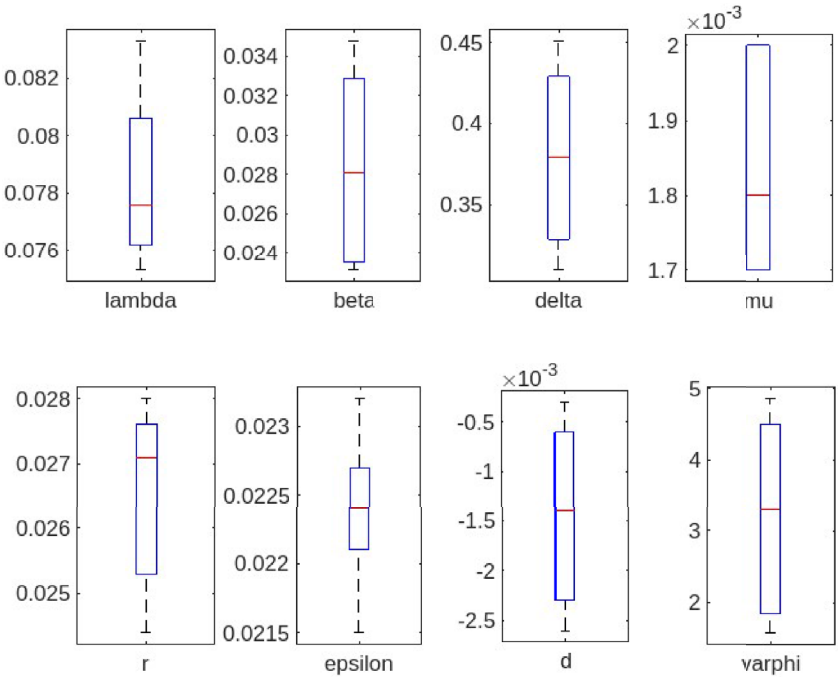

(a) 02 Feb to 01 Sept 2021

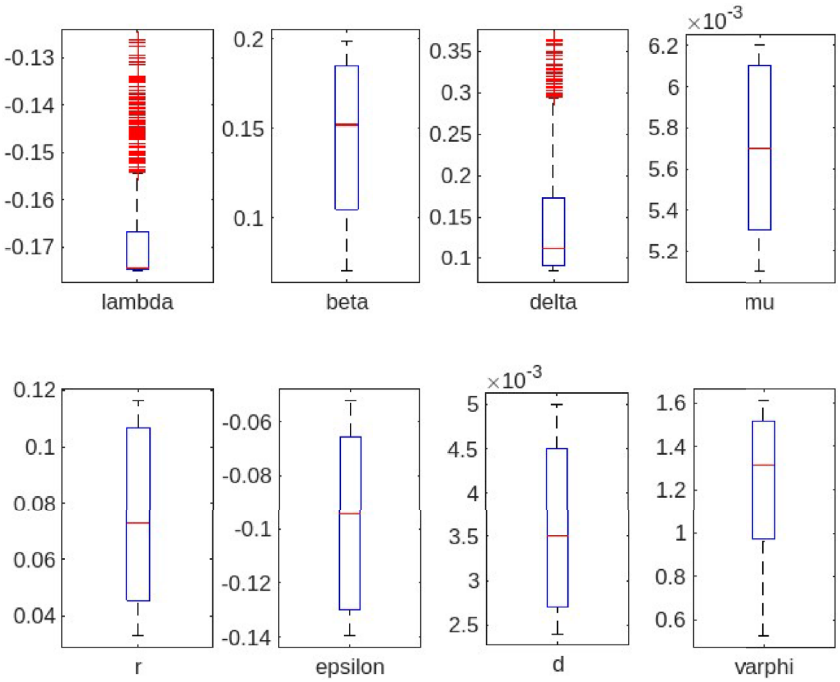

(b) 02 Sept to 29 Nov 2021

Fig. 11 Box-plot for all parameters $(\lambda, \beta, \delta, \mu, r, \epsilon, d, \varphi)$ with the range (02 Feb to 01 Sept 2021) and (02 Sept to 29 Nov 2021)

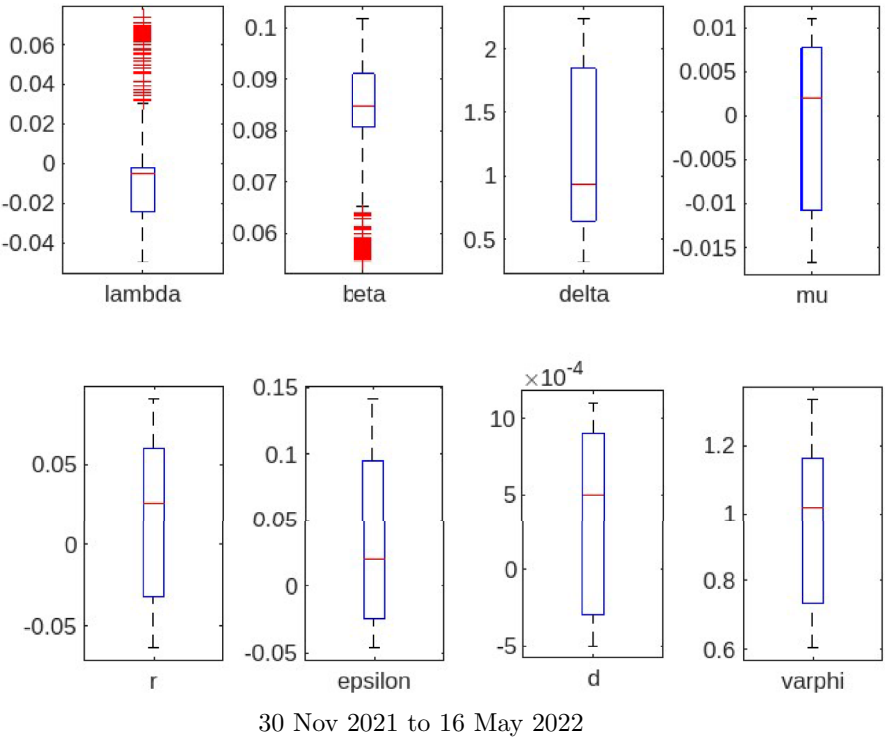

Fig. 12 Box-plot for all parameters $(\lambda, \beta, \delta, \mu, r, \epsilon, d, \varphi)$ with the range (30 Nov 2021 to 16 May 2022)

Table 2 Best fit estimation of parameters for *SIQR* model and actual data CoVid-19

Parameter	Initial Guess	Fig. 9a	Fig. 9b	Fig. 9c	Fig. 9d	Fig. 9e
Λ	0.07	0.0748	−0.0145	0.0761	−0.1750	−0.0076
β	0.057	0.0847	0.0250	0.0348	0.1968	0.0775
δ	0.4	1.1354	2.7125	0.3089	0.0849	2.1788
μ	0.0019	0.0240	−0.0327	0.0017	0.0051	−0.0170
r	0.057	−0.0531	0.2299	0.0276	0.0351	0.0581
ϵ	0.03	−0.1449	−0.1449	0.0227	−0.0545	0.1395
d	0.001	−0.0342	0.0066	−0.0026	0.0024	−0.0010
φ	0.7	19.4606	6.4821	4.8535	1.5934	0.0826

Table 3 Dynamics of infected profiles for time 0, 50, 100, and 150

Time	Fig. 9a	Fig. 9b	Fig. 9c	Fig. 9d	Fig. 9e
0	0.0199	0.1963	0.3305	0.9411	0.0028
50	0.0379	0.1896	0.1029	0.1069	0.0158
100	0.3412	0.3228	0.1737	0.0001	0.1460
150	0.1850	0.3329	1.0259	0	0.0020
RMSE	6.17%	9.64%	28.68%	8.77%	14.13%

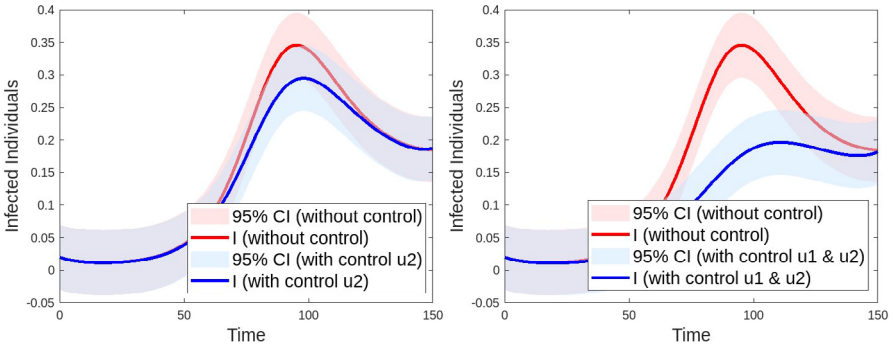

(a) Without Control versus With Control of Social Distancing (u_2)

(b) Without Control versus With Controls of Vaccination (u_1) and Social Distancing (u_2)

Fig. 13 Controls for estimation results with the actual data of infected individuals in range 09 Apr to 05 Sept 2020 (it refers to Fig. 9a)

Best Fit Parameters of *SIQR* Model

Now, we validate our dynamical system with the actual data by conducting the classical formula of least square technique written as

$$RMSE(\mathcal{N}) = \sum_{k=1}^{M} (\mathcal{Y}_{pred}(k) - \mathcal{Y}_{data}(k)), \tag{5.2}$$

where M is the number of actual data, $\mathcal{Y}_{pred}$ is the numerical result of our dyamical system, $\mathcal{Y}_{data}$ is the actual data of CoVid-19 in Semarang, Indonesia, taken from 09 Apr 2020 until to 16 May 2022, and $\mathcal{N}$ is the unknown parameters of our dynamical system in (2.1). Initially, the general form of our dynamical system (2.1) is represented as follows

$$\frac{d\mathcal{Y}(t)}{dt} = \mathcal{F}(t, \mathcal{Y}, \mathcal{N}), \tag{5.3}$$

where Eq. (5.3) is approximated by the iterative method, fourth order Runge–Kutta. Moreover, our goal is to minimize the objective function

$$\begin{aligned} &\min_{\mathcal{N}} \ RMSE(\mathcal{N}), \\ &\text{subject to Eq. (5.3).} \end{aligned} \tag{5.4}$$

The more detailed algorithm of parameter estimation can be addressed in [42] and the algorithm of optimization is in [32]. We divide the actual data into five parts: (a) Part 1 in Fig. 9a, (b) Part 2 in Fig. 9b, (c) Part 3 in Fig. 9c, (d) Part 4 in Fig. 9d, and (e) Part 5 in Fig. 9e, where each part has the peak values for number of infection. Moreover, Table 2 represents the best fit estimation values of parameters between *SIQR* model and actual data of CoVid-19 in Semarang, Indonesia, where the smallest RMSE (6.17%) is achieved in Fig. 9a, and the highest RMSE (28.68%) is provided in Fig. 9c as shown in Table 3 indicating the difference for each state (S, I, Q, R) between ODE45 results (based on the fitted parameters) and actual data. Moreover, Figs. 10, 11 and 12 provide the distribution of fitted parameters with actual data, where the highest number of outlier is shown in Fig. 11b for

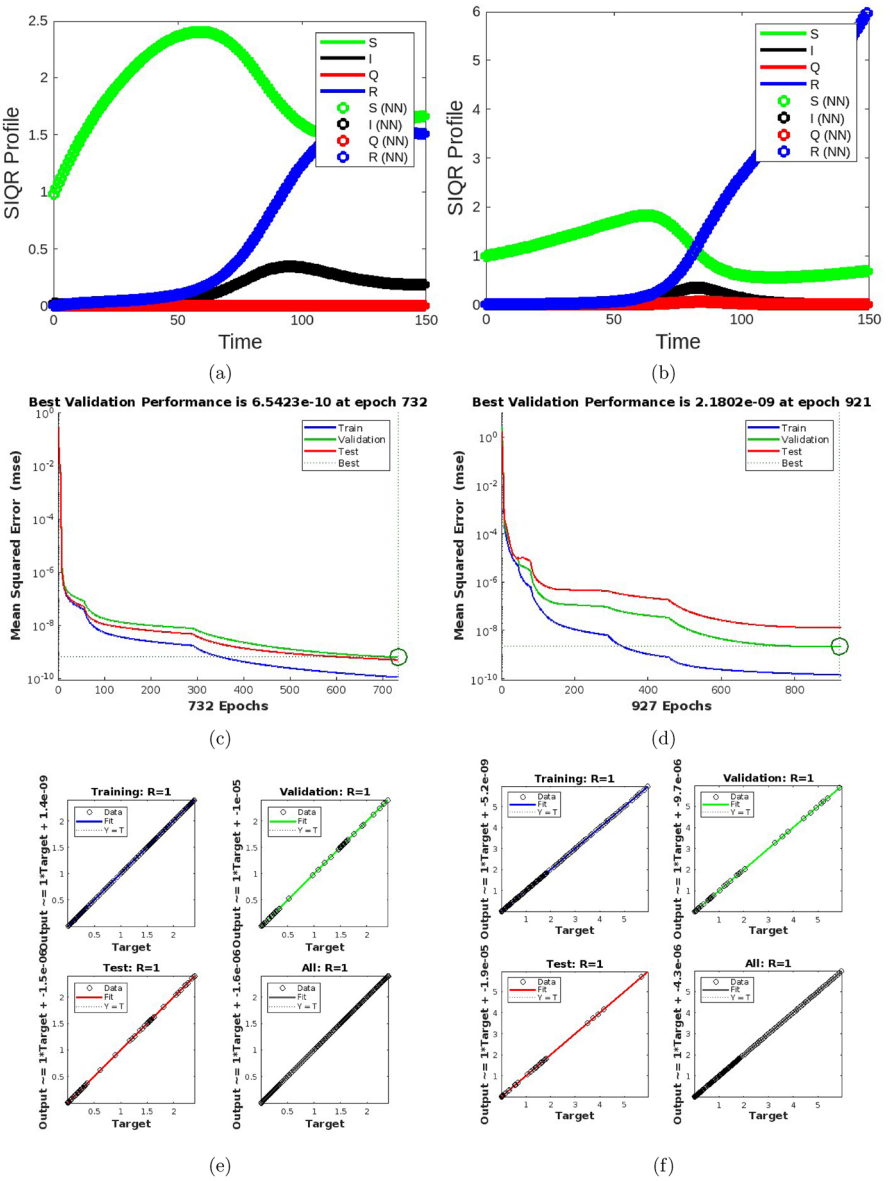

Fig. 14 **a**, **b** Estimation of neural network, **c**, **d** Performance, and **e**, **f** Regression for actual data as in Fig. 9a (LHS) and in Fig. 9e (RHS)

the parameter of λ. The parameters of $\mu, \epsilon, \delta, \mu$ do not provide the outlier and the obtained box-plots are mostly asymmetrical for each range.

Moreover, Fig. 4e, f and Fig. 5e, f provide the deterministic and stochastic of *SIQR* model of (2.1). The stochastic process are employed to describe the dynamical system for each event [5]. Initially, the dynamical system (2.1) is written as follows

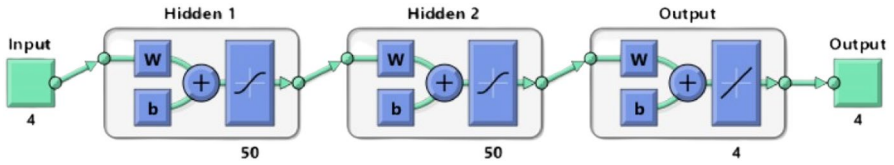

Fig. 15 Architecture of neural network consisting of 2 hidden layers, 50 neurons, training function of Levenberg-Marquardt, and activation function of Tangent Sigmoid

Table 4 The root mean square error between least square and neural network for the range of actual data from (09 Apr to 05 Sept 2020) and (30 Nov 2021 to 16 May 2022) for time 10, 20, 30, 40, 50, 60, 70, 80, 90, and 100

09 Apr to 05 Sept 2020				30 Nov 2021 to 16 May 2022			
S	*I*	*Q*	*R*	*S*	*I*	*Q*	*R*
0.000074	0.000001	0.000001	0.000019	0.000210	0.000003	0.000025	0.000006
0.000217	0.000005	0.000005	0.000007	0.000093	0.000003	0.000016	0.000013
0.000055	0.000055	0.000003	0.000067	0.001091	0.000020	0.000011	0.000108
0.000679	0.000087	0.000001	0.000177	0.000794	0.000016	0.000008	0.000026
0.000517	0.000034	0.000004	0.000045	0.000696	0.000054	0.000009	0.000202
0.000145	0.001133	0.000010	0.001991	0.000053	0.000041	0.000009	0.000059
0.002627	0.001608	0.000023	0.003192	0.000426	0.000434	0.000042	0.002241
0.002284	0.000898	0.000011	0.002549	0.002412	0.000433	0.000080	0.003219
0.002706	0.000477	0.000005	0.003498	0.001297	0.000573	0.000062	0.003484
0.001658	0.000249	0.000000	0.002918	0.000416	0.000497	0.000093	0.002752

$$\frac{d}{dt}X(\tau, x_0) = F(X(\tau, x_0)), \tag{5.5}$$

where F is Lipschitz continuous, and X is state space, for $X = (S, I, Q, R)$, and $X(0, x_0) = X_0$. By employing the limit $N \to +\infty$, the sequence of state space $X_N(0, x_0) = X_0$ and for every $\delta > 0$ the stochastic process is closed to the deterministic process as shown as follows

$$Pr\left(\sup_{t\leq\tau} |X_N(t) - X(t, x_0)| > \varepsilon\right) \to 0, \text{ as } N \to +\infty, \text{ for every } t \geq 0, \text{ and } \varepsilon > 0,$$

implying that the sequence of state space $(X_N(t),\ t \geq 0)$ can be approximated by the first order ordinary differential equations in Eq. (5.5). We notice that the function F is summation of a continuous function $f(X, L)$, where $f(X, L) : \mathbb{R}^4 \times \mathbb{Z}^4 \to \mathbb{R}$ and it is called as the process jumps for each event L. It follows from system (2.1), the process jumps are given below

$$f(X,L) = \begin{cases} \beta\delta SI, & L = (-1,1,0,0), \\ rI, & L = (0,-1,0,1), \\ \epsilon I, & L = (0,-1,1,0), \\ \varphi Q, & L = (0,0,-1,1), \\ \mu S, & L = (-1,0,0,0). \end{cases} \quad f(X,L) = \begin{cases} (\mu+d)I, & L = (0,-1,0,0), \\ (\mu+d)Q, & L = (0,0,-1,0), \\ \mu R, & L = (0,0,0,-1), \\ \Lambda, & L = (1,0,0,0). \end{cases}$$

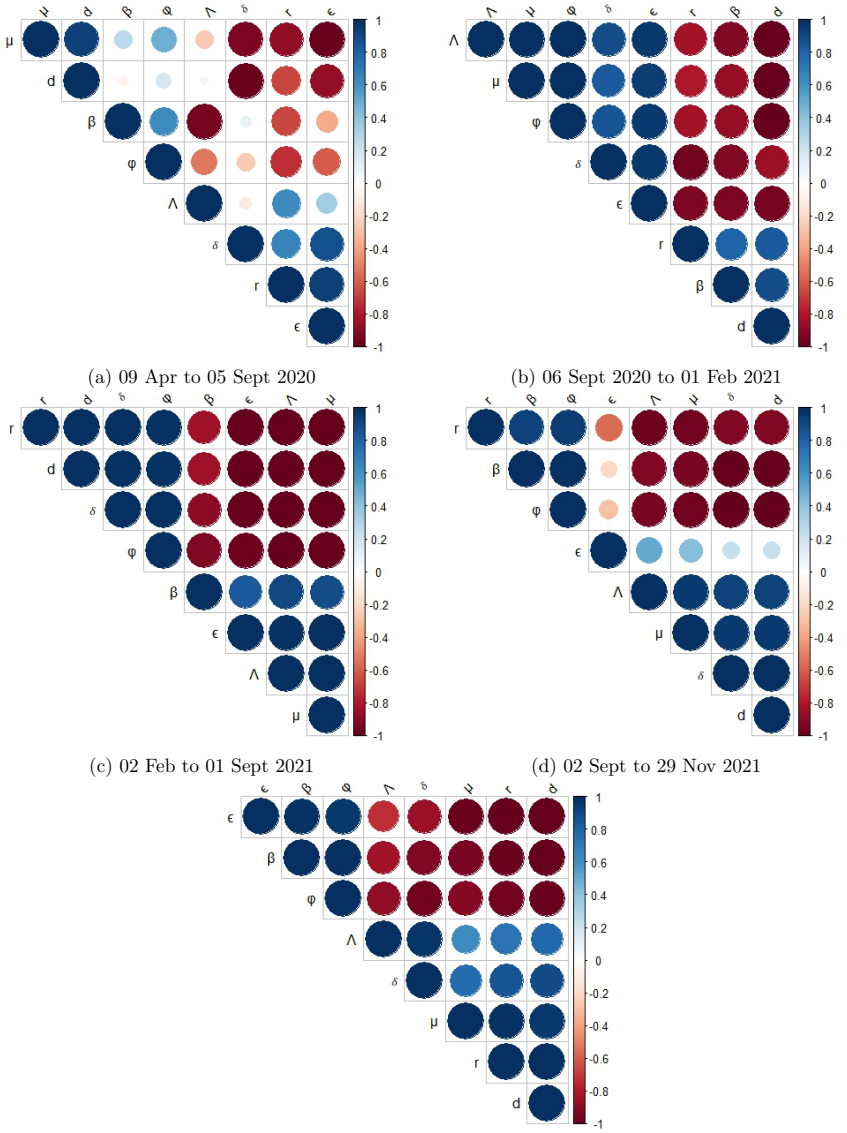

(a) 09 Apr to 05 Sept 2020

(b) 06 Sept 2020 to 01 Feb 2021

(c) 02 Feb to 01 Sept 2021

(d) 02 Sept to 29 Nov 2021

(e) 30 Nov 2021 to 16 May 2022

Fig. 16 Correlation matrix between two parameters

As in Figs. 4e, f and 5e, f, we can conclude that the deterministic and stochastic results give the same patterns for the profiles of susceptible, infected, quarantined, and recovered individuals. By referring to Fig. 13, we provide the control profiles for the estimation results with the actual data of infected individuals only in range (09 Apr to 05 Sept 2020) as the representation of five possible ranges as shown in Fig. 9. It can be seen that after applying the controls (only control of social distancing and after that using two controls of vaccination and social distancing), the infected profiles are more sloping than before applying the

Table 5 Numerical values of correlation matrix between two parameters X and Y ($Corr(X, Y)$)

Date	$Corr(X, Y)$	Λ	β	δ	μ	r	ϵ	d	φ
09 Apr to 05 Sept 2020	Λ	1.00	−0.96	−0.11	−0.25	0.64	0.34	0.06	−0.52
	β	−0.96	1.00	0.10	0.27	−0.67	−0.37	−0.07	0.63
	δ	−0.11	0.10	1.00	−0.93	0.66	0.88	−0.99	−0.25
	μ	−0.25	0.27	−0.93	1.00	−0.89	−0.99	0.93	0.49
	r	0.64	−0.67	0.66	−0.89	1.00	0.94	−0.66	−0.73
	ϵ	0.34	−0.37	0.88	−0.99	0.94	1.00	−0.87	−0.61
	d	0.06	−0.07	−0.99	0.93	−0.66	−0.87	1.00	0.18
	φ	−0.52	0.63	−0.25	0.49	−0.73	−0.61	0.18	1.00
06 Sept 2020 to 01 Feb 2021	Λ	1.00	−0.92	0.88	0.99	−0.83	0.97	−0.99	0.99
	β	−0.92	1.00	−0.93	−0.87	0.80	−0.93	0.88	−0.88
	δ	0.88	−0.93	1.00	0.83	−0.96	0.96	−0.86	0.85
	μ	0.99	−0.87	0.83	1.00	−0.81	0.94	−1.00	1.00
	r	−0.83	0.80	−0.96	−0.81	1.00	−0.93	0.83	−0.83
	ϵ	0.97	−0.93	0.96	0.94	−0.93	1.00	−0.96	0.96
	d	−0.99	0.88	−0.86	−1.00	0.83	−0.96	1.00	−1.00
	φ	0.99	−0.88	0.85	1.00	−0.83	0.96	−1.00	1.00
02 Feb to 01 Sept 2021	Λ	1.00	0.90	−1.00	1.00	−0.99	0.99	−0.99	−1.00
	β	0.90	1.00	−0.89	0.88	−0.84	0.83	−0.85	−0.93
	δ	−1.00	−0.89	1.00	−1.00	0.99	−0.99	1.00	1.00
	μ	1.00	0.88	−1.00	1.00	−1.00	1.00	−1.00	−0.99
	r	−0.99	−0.84	0.99	−1.00	1.00	−1.00	1.00	0.98
	ϵ	0.99	0.83	−0.99	1.00	−1.00	1.00	−1.00	−0.98
	d	−0.99	−0.85	1.00	−1.00	1.00	−1.00	1.00	0.98
	φ	−1.00	−0.93	1.00	−0.99	0.98	−0.98	0.98	1.00
02 Sept to 29 Nov 2021	Λ	1.00	−0.92	0.92	0.95	−0.98	0.51	0.92	−0.94
	β	−0.92	1.00	−1.00	−0.95	0.92	−0.21	−1.00	0.99
	δ	0.92	−1.00	1.00	0.96	−0.92	0.23	1.00	−1.00
	μ	0.95	−0.95	0.96	1.00	−0.96	0.42	0.96	−0.97
	r	−0.98	0.92	−0.92	−0.96	1.00	−0.57	−0.92	0.95
	ϵ	0.51	−0.21	0.23	0.42	−0.57	1.00	0.23	−0.29
	d	0.92	−1.00	1.00	0.96	−0.92	0.23	1.00	−1.00
	φ	−0.94	0.99	−1.00	−0.97	0.95	−0.29	−1.00	1.00
30 Nov 2021 to 16 May 2022	Λ	1.00	−0.83	0.97	0.62	0.73	−0.74	0.78	−0.89
	β	−0.83	1.00	−0.93	−0.95	−0.99	0.99	−1.00	0.99
	δ	0.97	−0.93	1.00	0.77	0.86	−0.86	0.89	−0.96
	μ	0.62	−0.95	0.77	1.00	0.99	−0.98	0.97	−0.91
	r	0.73	−0.99	0.86	0.99	1.00	−1.00	1.00	−0.96
	ϵ	−0.74	0.99	−0.86	−0.98	−1.00	1.00	−1.00	0.97
	d	0.78	−1.00	0.89	0.97	1.00	−1.00	1.00	−0.98
	φ	−0.89	0.99	−0.96	−0.91	−0.96	0.97	−0.98	1.00

controls. If we compare for both figures (Fig. 13a, b), we can conclude that applying two controls (vaccination and social distancing) at once is more sloping than only applying one control (social distancing). It indicates that applying two controls can effectively reduce the number of infected individuals for CoVid-19 disease in Semarang, Indonesia.

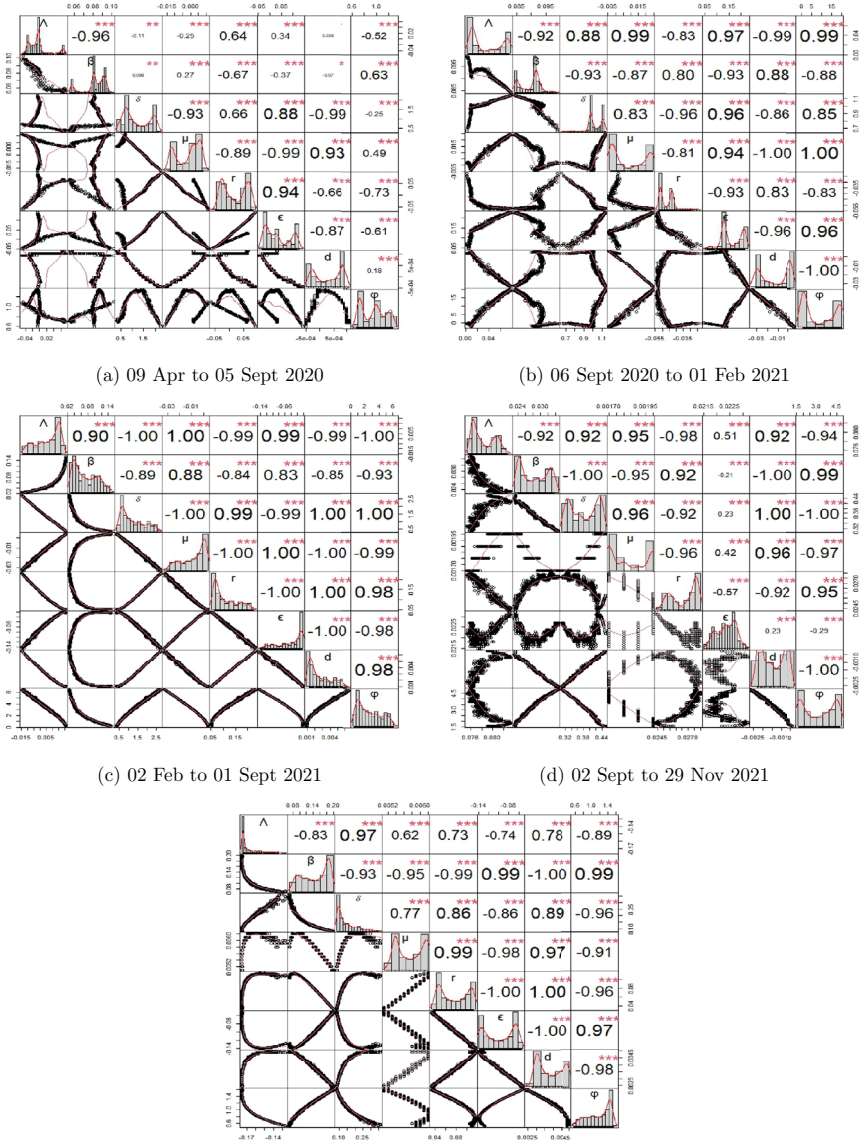

(a) 09 Apr to 05 Sept 2020

(b) 06 Sept 2020 to 01 Feb 2021

(c) 02 Feb to 01 Sept 2021

(d) 02 Sept to 29 Nov 2021

(e) 30 Nov 2021 to 16 May 2022

Fig. 17 Performance analytics between two parameters

Applying the same strategy as in [29] and based on the results of Fig. 9a, e, we propose the neural network to estimate the infected profile of CoVid-19 in Semarang Indonesia and the results are respectively obtained for the S, I, Q, R profiles, performance and regression as shown in Fig. 14. The left hand side (LHS) needs 732 epochs and the right hand side (RHS) needs 921 epochs to achieve the optimal conditions. Moreover, the regression results for both RHS and LHS provide the distribution data which is still on the track (for the correlations between training and testing). To achieve these all optimal results,

the architecture of neural network proposes two hidden layers consisting of 50 neurons for each hidden layer. Moreover, we employ Levenberg-Marquadt and Tangent Sigmoid as the training and activation functions respectively as in Fig. 15. According to the root mean square error for the profile of S, I, Q, R (between least square and neural network), one can conclude that the estimation results by using neural network are very significant as shown in Table 4.

The correlation between two parameters (based on the actual data of Covid-19 in Semarang, Indonesia from 09 Apr 2020 to 16 May 2022) is represented as the matrix correlation as shown in Fig. 16. Positive correlations are displayed in blue and negative correlations in red color. Color intensity and the size of the circle are proportional to the correlation coefficients. In the right side of the correlogram, the legend color shows the correlation coefficients and the corresponding colors. Based on the matrix correlation, the smallest correlation size is the correlation between (d and λ indicating the small circle) for the range (09 Apr to 05 Sept 2020). Meanwhile, two ranges of (06 Sept 2020 to 01 Feb 2021) and (02 Feb to 01 Sept 2021) provide the same size circle (indicating the correlation size) for almost all correlations among the parameters. If we compare these two matrix correlations with the box-plot as in Fig. 12, there is no outlier for two ranges of (06 Sept 2020 to 01 Feb 2021) and (02 Feb to 01 Sept 2021), where all numerical values of Fig. 16 are shown in Table 5 and the performance analytics are in Fig. 17. The distribution of each parameter is shown on the diagonal. On the bottom of the diagonal, the bivariate scatter plots with a fitted line are displayed. On the top of the diagonal, the value of the correlation plus the significance level as stars Each significance level is associated to a symbol, i.e., p-values(0.001, 0.01, 0.05, 0.1, 1) refer to symbols("***", "**", "*", ".", " ").

Conclusion

The mathematical model of CoVid-19 with optimal control of vaccination and social distancing becomes our concern in this paper. The aim of control implementation is to reduce the number of infected individuals. Based on the results obtained in the numerical simulation, those two controls give a significant effect on a dynamical system for each variable state. The local stability is established by analyzing the stability characteristic through the Jacobian matrix at the disease-free and endemic disease equilibrium points. Moreover, the global stability issue is from the appropriate Lyapunov function. The least-square technique is employed to provide the validation of our dynamical system by comparing the numerical results using fourth-order Runge Kutta and actual data of CoVid-19 disease in Semarang, Indonesia. As in the results obtained, our model of a dynamical system is good enough for the estimation based on the RMSE values. By employing the Continuous Time Markov Chain (CTMC), we have the same patterns for the profiles of susceptible, infected, quarantined, and recovered individuals between the deterministic and stochastic results. Applying two controls (vaccination and social distancing) at once is more effective than only applying one control (social distancing) to reduce the number of infected individuals for CoVid-19 in Semarang, Indonesia. According to the discussions, it can be seen that the infected profile of two controls at once (vaccination and social distancing) is more sloping than the infected profile of only one control (social distancing). The neural network technique also gives the significant estimations based on the root mean square error by using the training function of Levenberg-Marquadt and activation function of Tangent Sigmoid consisting of two hidden layers and 50 neurons for each hidden layer.

Appendix: Source Code of Continuous Time Markov Chain

```
%function
function f = sir_rhs_3(t,y,pars)
f=zeros(4,1);
f(1)=pars(1)-pars(2)*pars(3)*y(1)*y(2)-pars(4)*y(1);
f(2)=pars(2)*pars(3)*y(1)*y(2)-(pars(5)+pars(6)+pars(4)+pars(7))*y(2);
f(3)=pars(6)*y(2)-(pars(8)+pars(7)+pars(4))*y(3);
f(4)=pars(5)*y(2)+pars(8)*y(3)-pars(4)*y(4);
end
%main program
clear all;clc;close all
beta=0.01;
lambda=0.01;
delta=1;
mu=0.00003;
r_param=0.03;
epsilon=0.025;
d=0.008;
psi=0.04;
N=100;
s0=98;
i0=2;
r0=0;
q0=0;
tm=20;
sim=3;
for k=1:sim
t(1)=0;
i(1)=i0;
s(1)=s0;
q(1)=q0;
r(1)=r0;
j=1;
while i(j)>0 & t(j)<tm
u1=rand(); % uniform random number
u2=rand(); % uniform random number
a1=beta*delta*s(j)*i(j);
a2=r_param*i(j);
a3=epsilon*i(j);
a4=psi*q(j);
a5=mu*s(j);
a6=(mu+d)*i(j);
a7=(mu+d)*q(j);
a8=mu*r(j);
a9=lambda;
den=a1+a2+a3+a4+a5+a6+a7+a8;
t(j+1)=-log(u1)/den+t(j) % Time to next event
e1=a1/den;
e2=e1+a2/den;
e3=e2+a3/den;
e4=e3+a4/den;
e5=a4+a5/den;
e6=e5+a6/den;
e7=e6+a7/den;
e8=e7+a8/den;
e9=e8+a9/den;
if (u2<=e1)
s(j+1)=s(j)-1;
i(j+1)=i(j)+1;
q(j+1)=q(j);
r(j+1)=r(j);
elseif (u2>e1 & u2<=e2)
s(j+1)=s(j);
```

```
i(j+1)=i(j)-1;
q(j+1)=q(j);
r(j+1)=r(j)+1;
elseif (u2>e2 & u2<=e3)
s(j+1)=s(j);
i(j+1)=i(j)-1;
q(j+1)=q(j)+1;
r(j+1)=r(j);
elseif (u2>e3 & u2<=e4)
s(j+1)=s(j);
i(j+1)=i(j);
q(j+1)=q(j)-1;
r(j+1)=r(j)+1;
elseif (u2>e4 & u2<=e5)
s(j+1)=s(j)-1;
i(j+1)=i(j);
q(j+1)=q(j);
r(j+1)=r(j);
elseif (u2>e5 & u2<=e6)
s(j+1)=s(j);
i(j+1)=i(j)-1;
q(j+1)=q(j);
r(j+1)=r(j);
elseif (u2>e6 & u2<=e7)
s(j+1)=s(j);
i(j+1)=i(j);
q(j+1)=q(j)-1;
r(j+1)=r(j);
elseif (u2>e7 & u2<=e8)
s(j+1)=s(j);
i(j+1)=i(j);
q(j+1)=q(j);
r(j+1)=r(j)-1;
else
s(j+1)=s(j)+1;
i(j+1)=i(j);
q(j+1)=q(j);
r(j+1)=r(j);
end
j=j+1;
end
plot(t,s,'b-',t,i,'r-',t,q,'g-',t,r,'k-','LineWidth',1)
hold on
end
%%
tF=20;
t = linspace(0, tF, 2001)+.1;
y0=[s0;i0;q0;r0];
% Run ODE
[t,y] = ode45(@sir_rhs_3,t,y0,[],[lambda,beta,delta,mu,r_param,epsilon,d,psi,N]);
plot(t,y(:,1),'b-',t,y(:,2),'r-',t,y(:,3),'g-',t,y(:,4),'k-','LineWidth',2.4)
h=legend('S (\epsilon-0.5%)','I (\epsilon-0.5%)','Q (\epsilon-0.5%)','R (\epsilon-0.5%)');
set(h,'FontSize',14);
ylabel('(S,I,Q,R)(t)','FontSize',14)
xlabel('Time','FontSize',14)
xlim([0 20])
```

Acknowledgements The authors would like to thank the reviewers for their valuable comments and suggestions which helped to improve the paper. There are no funders to report for this submission.

Data Availability The actual data can be accessed online through the following link: https://siagacorona.semarangkota.go.id/halaman/covid19pertahun/2020.

Declarations

Conflict of interest This work does not have any conflicts of interest.

Use of AI tools declaration The authors declare no use of Artificial Intelligence (AI) tools in the creation of this paper.

References

1. Adnan, et al.: Investigation of time-fractional SIQR Covid-19 mathematical model with fractal-fractional Mittage-Leffler kernel. Alexandria Eng. J. **61**(10), 7771–7779 (2022). https://doi.org/10.1016/j.aej.2022.01.030
2. Ahmed, N., Raza, A., Rafiq, M., Ahmadian, A., Batool, N., Salahshour, S.: Numerical and bifurcation analysis of SIQR model. Chaos Solit. Fract. **150**, 111133 (2021). https://doi.org/10.1016/j.chaos.2021.111133
3. Alenezi, M.N., Al-Anzi, F.S., Alabdulrazzaq, H.: Building a sensible SIR estimation model for COVID-19 outspread in Kuwait. Alexandria Eng. J. **60**(3), 3161–3175 (2021). https://doi.org/10.1016/j.aej.2021.01.025
4. Alqahtani, R.T.: Mathematical model of SIR epidemic system (COVID-19) with fractional derivative: stability and numerical analysis. Adv. Differ. Equ. **1**, 2021 (2021). https://doi.org/10.1186/s13662-020-03192-w
5. Allen, L.J.S.: Modeling with Itô Stochastic Differential Equations. Springer, Dordrecht (2007)
6. Al-Raeei, M.: The basic reproduction number of the new coronavirus pandemic with mortality for India, the Syrian Arab Republic, the United States, Yemen, China, France, Nigeria and Russia with different rate of cases. Clin. Epidemiol. Glob. Heal., vol. 9, no. August 2020, pp. 147-149, (2021), https://doi.org/10.1016/j.cegh.2020.08.005
7. Alshammari, F.S., Khan, M.A.: Dynamic behaviors of a modified SIR model with nonlinear incidence and recovery rates. Alexandria Eng. J. **60**(3), 2997–3005 (2021). https://doi.org/10.1016/j.aej.2021.01.023
8. Annas, S., Isbar Pratama, M., Rifandi, M., Sanusi, W., Side, S.: Stability analysis and numerical simulation of SEIR model for pandemic COVID-19 spread in Indonesia. Chaos Solit. Fract. **139**, 110072 (2020). https://doi.org/10.1016/j.chaos.2020.110072
9. Ariffin, M.R.K., et al.: Mathematical epidemiologic and simulation modelling of first wave COVID-19 in Malaysia. Sci. Rep. **11**(1), 1–10 (2021). https://doi.org/10.1038/s41598-021-99541-0
10. Atangana, A., Igret Araz, S.: Mathematical model of COVID-19 spread in Turkey and South Africa: theory, methods, and applications. Advances in Difference Equations., vol. 659, (2020). https://doi.org/10.1186/s13662-020-03095-w
11. Atangana, A., Igret Araz, S.: Modeling and forecasting the spread of COVID-19 with stochastic and deterministic approaches: Africa and Europe. Advances in Difference Equations., vol. 57, (2021), https://doi.org/10.1186/s13662-021-03213-2
12. Calafiore, G.C., Novara, C., Possieri, C.: A time-varying SIRD model for the COVID-19 contagion in Italy. Annu. Rev. Control. **50**(October), 361–372 (2020). https://doi.org/10.1016/j.arcontrol.2020.10.005
13. Cartocci, A., Cevenini, G., Barbini, P.: A compartment modeling approach to reconstruct and analyze gender and age-grouped CoViD-19 Italian data for decision-making strategies. J. Biomed. Inform., vol. 118, no. April, p. 103793 (2021). https://doi.org/10.1016/j.jbi.2021.103793
14. Carvalho, D., Barbastefano, R., Pastore, D. et al.: A novel predictive mathematical model for CoVid-19 pandemic with quarantine, contagion dynamics, and environmentally mediated transmission. MedRxiv (2020)
15. Cao, Z., Feng, W., Wen, X., Zu, L., Cheng, M.: Dynamics of a stochastic SIQR epidemic model with standard incidence. Phys. A Stat. Mech. Appl. **527**, 1–12 (2019). https://doi.org/10.1016/j.physa.2019.121180
16. Chavez, C.C., Feng, Z., Huang, W.: On the computation of R^0 and its role in global stability. IMA Vol. Math. Appl. **125**, 29–50 (2002)

17. Chu, Y.M., Ali, A., Khan, M.A., Islam, S., Ullah, S., Higazy, M.: Dynamics of fractional order COVID-19 model with a case study of Saudi Arabia. Results in Physics., vol. 21 (2021). https://doi.org/10.1016/j.rinp.2020.103787
18. Chu, Y.M., Rashid, S., Akdemir, A.O., Khalid, A., Baleanu, D., Al-Sinan, B.R., Elzibar, O.A.I.: Predictive dynamical modeling and stability of the equilibria in a discrete fractional difference COVID-19 epidemic model. Results Phys. vol. 49 (2023). https://doi.org/10.1016/j.rinp.2023.106467
19. Chu, Y.M., Sultana, S., Rashid, S., Alharthi, M.S., Higazy, M.: Dynamical analysis of the stochastic COVID-19 model using piecewise differential equation technique. Comput. Model. Eng. Sci. **137**, 2427–2464 (2023). https://doi.org/10.32604/cmes.2023.028771
20. Chu, Y.M., Zarin, R., Khan, A., Murtaza, S.: A vigorous study of fractional order mathematical model for SARS-CoV-2 epidemic with Mittag-Leffler kernel. Alex. Eng. J. **71**, 565–579 (2023). https://doi.org/10.1016/j.aej.2023.03.037
21. Crokidakis, N.: CoVid-19 spreading in Rio de Janeiro, Brazil: Do the policies of social isolation really work? Chaos Solit. Fract. **136**, 109930 (2020). https://doi.org/10.1016/j.chaos.2020.109930
22. Crokidakis, N.: Modeling the early evolution of the CoVid-19 in Brazil; results from a Susceptible-Infectious-Quarantined-Recovered (SIQR). Int. J. Mod. Phys. C **31**, 1–8 (2020). https://doi.org/10.1142/S0129183120501351
23. Cooper, I., Mondal, A., Antonopoulos, C. G.: A SIR Model Assumption for The Spread of COVID-19 in Different Commnities. Chaos Solit. Fract. **139**, 110057 (2020). https://doi.org/10.1016/j.chaos.2020.110057
24. Demongeot, J., Griette, Q., Magal, P.: SI epidemic model applied to COVID-19 data in mainland China. R. Soc. Open Sci., vol. 7, no. 12 (2020). https://doi.org/10.1098/rsos.201878
25. Djalante, R., et al.: Review and analysis of current responses to COVID-19 in Indonesia: Period of January to March 2020. Prog. Disaster Sci., vol. 6 (2020). https://doi.org/10.1016/j.pdisas.2020.100091
26. Fernandez, P. M., Fernandez-Muniz, Z., Cernea, A., Luis Fernandez-Martınez, J., Kloczkowski, A.: Comparison of three mathematical models for COVID-19 prediction. Biophys. J., vol. 122, no. 3S1 (2023). https://doi.org/10.1016/j.bpj.2022.11.1616
27. Fraser, C., Donnelly, C. A., Cauchemez, S., et al.: Pandemic Potential of a Strain of Influenza A (H1N1): Early Findings. Science. **324**, 1557–1561 (2009)
28. Fuady, A., Nuraini, N., Sukandar, K.K.: Targeted Vaccine Allocation Could Increase the COVID-19 Vaccine Benefits Amidst Its Lack of Availability, A Mathematical Modeling Study in Indonesia. Vaccines **9**, 462 (2021). https://doi.org/10.3390/vaccines9050462
29. Ghani, M.: Dynamics of spatio-temporal HIV-AIDS model with the treatments of HAART and immunotherapy. International Journal of Dynamics and Control, (2023) (In Press). https://doi.org/10.1007/s40435-023-01284-5
30. He, S., Peng, Y., Sun, K.: SEIR modeling of the COVID-19 and its dynamics. Nonlinear Dyn. **101**(3), 1667–1680 (2020). https://doi.org/10.1007/s11071-020-05743-y
31. Igret Araz, S.: Analysis of a Covid-19 model: Optimal control, stability and simulations. Alexandria Engineering Journal., vol. 60 (2021). https://doi.org/10.1016/j.aej.2020.09.058
32. Kristensen, M.R.: Parameter estimation in nonlinear dynamical systems Master's Thesis, Technical University of Denmark. Kongens (2014)
33. Kudryashov, N.A., Chmykhov, M.A., Vigdorowitsch, M.: Analytical features of the SIR model and their applications to COVID-19. Appl. Math. Model. **90**, 466–473 (2021). https://doi.org/10.1016/j.apm.2020.08.057
34. Mahase, E.: Covid-19: What do we know about XBB.1.5 and should we be worried?. BMJ, vol. 380, no. May, p. p153, (2023). https://doi.org/10.1136/bmj.p153
35. Marinov, T. T., Marinova, R. S.: Adaptive SIR model with vaccination, simultaneous identification of rates and functions illustrated with COVID - 19. Sci. Rep., pp. 1–13 (2022). https://doi.org/10.1038/s41598-022-20276-7
36. Martínez, V.: A modified sird model to study the evolution of the covid-19 pandemic in spain. Symmetry (Basel)., vol. 13, no. 4 (2021). https://doi.org/10.3390/sym13040723
37. Nanda, M. A., et al.: The susceptible-infected-recovered-dead model for long-term identification of key epidemiological parameters of COVID-19 in Indonesia. Int. J. Electr. Comput. Eng. **12**(3), 2900–2910 (2022). https://doi.org/10.11591/ijece.v12i3.pp2900-2910
38. Odagaki, T.: Analysis of the outbreak of COVID-19 in Japan by SIQR model. Infect. Dis. Model. **5**, 691–698 (2020). https://doi.org/10.1016/j.idm.2020.08.013
39. Pandey, P., Chu, Y.M., Gomez-Aguilar, J.F., Jahanshahi, H., Alay, A.A.: A novel fractional mathematical model of COVID-19 epidemic considering quarantine and latent time. Results in Physics., vol. 26, (2021), https://doi.org/10.1016/j.rinp.2021.104286

40. Parhusip, H. A., Trihandaru, S., Wicaksono, B. A. A., Indrajaya, D., Sardjono, Y., Vyas, O. P.: Susceptible Vaccine Infected Removed (SVIR) Model for COVID-19 Cases in Indonesia. Sci. Technol. Indones. **7**(3), 400–408 (2022). https://doi.org/10.26554/sti.2022.7.3.400-408
41. Pontryagin, L., Boltyanskii, V., Gamkrelidze, R., et al.: The Mathematical Theory of Optimal Processes. Wiley, NY (1962)
42. Samsuzzoha, M., Singh, M., Lucy, D.: Parameter estimation of influenza epidemic model. Appl. Math. Comput. 220–616 (2013)
43. Sepulveda, G., Arenas, A.J., González-Parra, G.: Mathematical modeling of COVID-19 dynamics under two vaccination doses and delay effects. Mathematics **11**(2), 1–30 (2023). https://doi.org/10.3390/math11020369
44. Shen, Z.H., Chu, Y.M., Khan, M.A., Muhammad, S., Al-Hartomy, O.A., Higazy, M.: Mathematical modeling and optimal control of the COVID-19 dynamics. Results Phys. vol. 31 (2021). https://doi.org/10.1016/j.rinp.2021.105028
45. ud Din, R., Algehyne, E. A.: Mathematical analysis of COVID-19 by using SIR model with convex incidence rate. Results Phys. **23**, 1–6 (2021). https://doi.org/10.1016/j.rinp.2021.103970